



HAL
open science

The parasitophorous vacuole nutrient channel is critical for drug access in malaria parasites and modulates the artemisinin resistance fitness cost

Paolo Mesén-Ramírez, Bärbel Bergmann, Mourad Elhabiri, Lei Zhu, Heidrun von Thien, Carolina Castro-Peña, Tim-Wolf Gilberger, Elisabeth Davioud-Charvet, Zbynek Bozdech, Anna Bachmann, et al.

► To cite this version:

Paolo Mesén-Ramírez, Bärbel Bergmann, Mourad Elhabiri, Lei Zhu, Heidrun von Thien, et al.. The parasitophorous vacuole nutrient channel is critical for drug access in malaria parasites and modulates the artemisinin resistance fitness cost. *Cell Host & Microbe*, 2021, 29 (12), pp.1774-1787.e9. 10.1016/j.chom.2021.11.002 . hal-03544974

HAL Id: hal-03544974

<https://hal.science/hal-03544974>

Submitted on 12 Oct 2022

HAL is a multi-disciplinary open access archive for the deposit and dissemination of scientific research documents, whether they are published or not. The documents may come from teaching and research institutions in France or abroad, or from public or private research centers.

L'archive ouverte pluridisciplinaire **HAL**, est destinée au dépôt et à la diffusion de documents scientifiques de niveau recherche, publiés ou non, émanant des établissements d'enseignement et de recherche français ou étrangers, des laboratoires publics ou privés.

1 **The parasitophorous vacuole nutrient pore is critical for drug access in malaria parasites**
2 **and modulates the fitness cost of artemisinin resistance**

3

4 Paolo Mesén-Ramírez¹, Bärbel Bergmann¹, Mourad Elhabiri², Lei Zhu³, Heidrun von Thien^{1,4},
5 Carolina Castro-Peña¹, Tim-Wolf Gilberger^{1,4}, Elisabeth Davioud-Charvet², Zbynec
6 Bozdech^{3,5}, Anna Bachmann^{1,4}, Tobias Spielmann^{1,6}

7

8

9

10 ¹ Bernhard Nocht Institute for Tropical Medicine, Bernhard Nocht Str. 74, 20359 Hamburg,
11 Germany.

12 ² UMR7042 Université de Strasbourg–CNRS–UHA, Laboratoire d'Innovation Moléculaire et
13 Applications (LIMA), Team Bio(IN)organic and Medicinal Chemistry, European School of
14 Chemistry, Polymers and Materials (ECPM), 25 Rue Becquerel, F-67087 Strasbourg, France

15 ³ School of Biological Sciences, Nanyang Technological University, 60 Nanyang Drive,
16 Singapore 637551

17 ⁴ Centre for Structural Systems Biology, Notkestraße 85, Building 15, 22607, University of
18 Hamburg, 20146 Hamburg, Germany

19 ⁵ Honorary Visiting Research Fellow, Nuffield Department of Medicine, University of Oxford,
20 UK

21 ⁶ Lead contact

22

23

24

25

26 correspondence: spielmann@bni-hamburg.de

27

28

29

30

31

32 **Summary**

33 Intraerythrocytic malaria parasites proliferate bounded by a parasitophorous vacuolar
34 membrane (PVM). The PVM contains nutrient permeable channels (NPCs) conductive to small
35 molecules but their relevance for parasite growth for individual metabolites is largely
36 untested. Here we show that growth relevant levels of major carbon and energy sources pass
37 through the NPCs. Moreover, we find that the NPCs are a gate for several antimalarial drugs,
38 highlighting their permeability properties as a critical factor for drug design. Looking into NPC-
39 dependent amino acid transport, we find that amino acid shortage is a reason for the fitness
40 cost in artemisinin resistant (ART^R) parasites and provide evidence that NPC upregulation to
41 increase amino acids acquisition is a mechanism of ART^R parasites *in vitro* and in human
42 infections to compensate this fitness cost. Hence, the NPCs are important for nutrient and
43 drug access and reveal amino acid deprivation as a critical constraint in ART^R parasites.

44

45 **Introduction**

46 Malaria caused by *P. falciparum* parasites is responsible for more than 400,000 deaths every
47 year(WHO, 2019). The symptoms of malaria are caused by continuous cycles of parasite
48 multiplication in red blood cells (RBCs). During their intracellular development malaria
49 parasites propagate in a vacuolar compartment surrounded by the PVM(Lingelbach and
50 Joiner, 1998; Spielmann et al., 2012). The parasites establish nutrient permeable channels
51 (NPCs) at the PVM that are conductive to small molecules(Desai and Rosenberg, 1997).
52 Electrophysiological measurements with parasites extruded from the host cell and isolated
53 membranes demonstrated that the NPCs are mostly in an open state and show low selectivity
54 for molecules of 1.4 kDa or less(Desai et al., 1993; Desai and Rosenberg, 1997; Garten et al.,
55 2018). However, it is unclear for which metabolites this activity is growth relevant. Recent
56 work implicated the PVM proteins EXP2(Garten et al., 2018), EXP1(Mesen-Ramirez et al.,
57 2019) and RON3(Low et al., 2019) in NPC activity (NPCA). While EXP2 and RON3 are also
58 needed for protein export, inactivation of EXP1 specifically affects the NPCA without
59 interfering with protein export(Mesen-Ramirez et al., 2019; Nessel et al., 2020).

60

61 Reduced susceptibility of parasites to artemisinin derivatives (ART) (here simplified as 'ART-
62 resistance') and its partner drugs, such as piperaquine (PPQ), is now common in many regions

63 of South East Asia, causing treatment failures and hampering the efforts to control
64 malaria(Amaratunga et al., 2012; Dondorp et al., 2009; Duru et al., 2015; Leang et al., 2015;
65 Saunders et al., 2014; Witkowski et al., 2013; Woodrow and White, 2017). Upregulation of
66 *exp1* transcript levels has been observed in some resistant parasite lines(Lisewski et al., 2014;
67 Rocamora et al., 2018). It was postulated that EXP1 is a membrane glutathione transferase
68 (MGST) that detoxifies heme and has a role in ART resistance by protecting the parasites from
69 ART-mediated oxidative damage(Lisewski et al., 2014). However, recent work showed that
70 the proposed MGST catalytic site of EXP1 is not important for its function and no evidence
71 was found for EXP1 as a causal factor in ART resistance (Mesen-Ramirez et al., 2019; Nessel
72 et al., 2020). Diverse other transcriptional and metabolic alterations have been observed in
73 ART resistant (ART^R) parasites(Mok et al., 2015; Mok et al., 2011; Mok et al., 2021; Rocamora
74 et al., 2018; Siddiqui et al., 2017; Sutherland et al., 2020; Yang et al., 2019; Zhang et al., 2017).
75 However, the roles of these changes and of EXP1 in ART-resistance remain unclear.

76

77 Single point mutations in the propeller domain of the parasite's Kelch13 protein result in ART-
78 resistance(Ariey et al., 2014; Straimer et al., 2015) and such mutations have now also been
79 detected in Africa(Uwimana et al., 2020). Malaria parasites endocytose hemoglobin from the
80 host RBC and digest it in the food vacuole (FV), the parasite's lysosome-like organelle(Francis
81 et al., 1997; Spielmann et al., 2020), resulting in degradation products that activate ART(Klonis
82 et al., 2013). ART^R parasites show reduced hemoglobin endocytosis, leading to resistance,
83 likely due to reduced drug activation(Birnbaum et al., 2020; Yang et al., 2019). Resistance
84 involves only the first intra-erythrocytic phase, the ring stage(Witkowski et al., 2013), and is
85 associated with a fitness cost for the parasite(Nair et al., 2018; Straimer et al., 2017). The
86 reason for the fitness cost of ART resistance is unknown but we previously hypothesised that
87 it might be due to a reduced hemoglobin-derived amino acid supply in ring stages(Birnbaum
88 et al., 2020). Intra-erythrocytic malaria parasites obtain amino acids from two sources: the
89 proteolysis of the globin chains of the hemoglobin endocytosed from the RBC cytosol and free
90 amino acids from the human serum or culture medium(Babbitt et al., 2012; Liu et al., 2006).
91 The latter requires transport across the RBC membrane (Desai et al., 2000; Ginsburg et al.,
92 1983) and the PVM (Desai et al., 1993; Garten et al., 2018; Mesen-Ramirez et al., 2019) but
93 this transport route has not so far been analysed in ART^R parasites.

94

95 Here we exploited EXP1 mutants to analyse the function of the NPCA in the passage of small
96 solutes across the PVM to reach the parasite and the role of this process in ART^R parasites.
97 The results of this work provide evidence that amino acid deprivation is a reason for the
98 fitness cost in ART^R parasites and that *Plasmodium* parasites can compensate this fitness cost
99 by increasing EXP1 expression to elevate NPC-dependent acquisition of serum-derived amino
100 acids. These findings suggest that the reduced hemoglobin endocytosis in ART^R parasites has
101 profound downstream effects that include compensatory adaptations and may explain many
102 changes observed in these parasites.

103

104

105 **Results**

106 **Nutrients passing through the NPCs**

107 To study the NPCA we took advantage of previously established conditional *exp1* knock out
108 (KO) parasites that contain an additional copy of *exp1* expressed at low levels (Mesen-Ramirez
109 et al., 2019). Induction of the KO (+ rapalog) results in parasites relying on low levels of EXP1
110 derived from the additional copy (Figure 1A). These EXP1^{low} parasites show reduced NPCA
111 and are hypersensitive to low amino acid concentrations (Mesen-Ramirez et al., 2019). This
112 indicated that the passage of amino acids through the NPC is vital for *P. falciparum* blood
113 stages and that this genetic approach can be used to assess which nutrients reach the parasite
114 via the NPC and if passage of a particular nutrient through the NPC is relevant for parasite
115 growth.

116

117 To further characterise the relationship between EXP1 function and the NPCA we tested
118 whether parasites relying on different modified versions of EXP1 (containing mutations or
119 deletions) showed alterations in the NPCA (Figures 1A and 1C and Figure S1A-G). Besides
120 previously established complementation constructs (Mesen-Ramirez et al., 2019) we included
121 a construct with a single point mutation in the EXP1 transmembrane (TM) domain from
122 encoding glycine to the typical TM helix residue leucine (EXP1 TMmut^{G83L}) which was sufficient
123 to fully inactivate EXP1 (Figures 1B and S1H-J). Parasites depending on versions of EXP1 with
124 low complementation activity displayed an aberrant localization of EXP2 (as observed in the
125 EXP1 KO (Mesen-Ramirez et al., 2019)) and became more sensitive to amino acid deprivation
126 (Figures 1B and S1A-S1G). Linear regression analysis showed that the mis-distribution of EXP2

127 and the susceptibility to amino acid restriction correlated with the complementation-activity
128 of a given EXP1 version (Figures 1C and 1D). This provides evidence that EXP1 is a contributor
129 to the NPCA and that EXP1 activity directly influences the access of nutrients through the NPC.

130

131 Previous work indicated that the NPCs are permeable for monosaccharides(Desai and
132 Rosenberg, 1997; Garten et al., 2018; Tanabe, 1990). Malaria parasites require a continuous
133 supply of glucose during propagation within RBCs(Kirk et al., 1996; Woodrow et al., 2000).
134 EXP1^{low} parasites were hypersensitive to glucose restriction (Figure 1E), indicating that
135 glucose reaches the parasite via NPCs and that its NPC passage is required for efficient
136 parasite growth (Figure 1E). In contrast, EXP1^{low} parasites were not hypersensitive to low
137 concentrations of the essential primary purine precursor hypoxanthine(Asahi et al., 1996) or
138 the essential fatty acids oleic and palmitic acid (that must be scavenged from the host cell(Mi-
139 Ichi et al., 2007; Mitamura et al., 2000)), indicating that these nutrients do not rely on the
140 NPCs to cross the PVM (Figures 1F and 1G).

141

142 To confirm that our growth assay reflects NPC-dependent passage of the assayed nutrients
143 into the parasite, we used the fluorescently labelled glucose analogue 2-(N-(7-nitrobenz-2-
144 oxa-1,3-diazol-4-yl)amino)-2-deoxyglucose (2-NBDG)(Low et al., 2019; Yamada et al., 2007)
145 (Figure 1H) to directly monitor glucose uptake in EXP1^{low} parasites. EXP1^{low} rings or
146 trophozoites both took up less glucose than controls and EXP1 overexpression (EXP1^{high})
147 restored glucose uptake (Figures 1I, 1J and S1K-S1L). This is consistent with the results from
148 the growth assays under glucose restriction (Figure 1E) and indicated that the NPCs are
149 already active in ring stages.

150

151 **Drugs pass through the PVM NPC**

152 Given the limited specificity of the NPCs(Desai and Rosenberg, 1997) we tested their
153 relevance for access of antimalarial drugs to the parasite. For this we exposed EXP1^{low}
154 parasites to IC50^{96h} of different drugs and assessed whether this affected the relative
155 sensitivity of these parasites compared to controls. IC50^{96h} of the drugs were used to
156 maximise the possible growth difference in either direction. Compared to controls, EXP1^{low}
157 parasites showed a reduced susceptibility to the 4-aminoquinolines (4-AQ) chloroquine,
158 amodiaquine, and mefloquine (MFQ) as well as to dihydroartemisinin (DHA) (Figures 2A-2D

159 and S2A-S2D), suggesting that the NPC facilitate access of these drugs to the parasite. In
160 contrast, MMV007839, an inhibitor of the lactate transporter at the parasite plasma
161 membrane(Golldack et al., 2017), and epoxomicin, a proteasome inhibitor peptide, did not
162 require the NPC to reach the parasite (Figures 2E and 2F).

163

164 If the reduced susceptibility of EXP1^{low} parasites was due to a reduced access of molecules
165 across the PVM, a higher NPCA would be expected to render parasites more sensitive to NPC-
166 permeable drugs. In accordance, parasites overexpressing EXP1 (via an episomal Ty1-tagged
167 copy) became more sensitive to DHA and MFQ (Figure 2G). We also assessed the effect of
168 exposure to IC50^{96h} DHA in our different complementation lines (Figures 1B and S1A-S1G). In
169 accordance with Figure 2D, parasites relying on EXP1 versions with low activity were less
170 susceptible to DHA (Figures S2E-S2L) and the susceptibility to DHA correlated with the activity
171 of the EXP1 construct the parasites were relying on (Figure 2H). These findings indicated that
172 the amount of DHA reaching the parasite correlates with the level of activity of EXP1.

173

174 4-AQ derivatives accumulate in the FV, where they inhibit hemozoin formation(Foley and
175 Tilley, 1998) and DHA is activated in the FV by hemoglobin by-products(Klonis et al., 2013). It
176 is therefore possible that the passage of other molecules through the NPC indirectly
177 influences the action of these drugs (e.g. by changing drug activation or accumulation in the
178 FV). For instance, glucose depletion influences FV pH(Saliba et al., 2003), which affects drug
179 accumulation of some 4-AQ(Jida et al., 2017; Yayon et al., 1984). However, MFQ, which may
180 have a different mode and site of action than other 4-AQ(Cowman et al., 1994; Wong et al.,
181 2017), was still dependent on the NPCs in our assay (Figures 2C and S2A-S2B), arguing against
182 an indirect effect based on mode of action. To further assess indirect influences, we tested
183 lumefantrine, an aryl amino alcohol unrelated to 4-AQ but with a similar mode of
184 action(Combrinck et al., 2013; Cowell and Winzeler, 2019). Lumefantrine susceptibility was
185 not influenced by NPC levels (Figure 2I), suggesting that the reduced susceptibility for 4-AQ
186 in EXP1^{low} parasites is independent of indirect effects arising from the mode of action of these
187 drugs. To further explore this issue, we directly monitored uptake of a fluorescently labelled
188 CQ analogue (Fluo-CQ) that has similar properties to CQ(Jida et al., 2017) (Figure 2J).
189 Unexpectedly, the uptake of Fluo-CQ and accumulation in the FV was not affected in EXP1^{low}
190 parasites (Figures 2J, 2K and S3A) and in contrast to CQ there was also no reduced

191 susceptibility to Fluo-CQ in these parasites (Figure 2L), suggesting that Fluo-CQ crosses the
192 PVM independently of the NPC. A related fluorescent CQ analogue (CQ1-NBD) (Figure S3B)
193 that locates to the parasite cytosol behaved similarly to Fluo-CQ (Figures S3C-S3F). Addition
194 of the NBD group tethered to a hydrophobic spacer of 5 methylene groups (Figures 2J and
195 S3B-S3C) likely increased the lipophilicity and membrane permeability of these CQ analogues.
196 Since Fluo-CQ has the same mode and site of action as CQ but does not depend on the NPC
197 to reach the parasite, this further supports that our growth assay measures the permeability
198 of the analysed 4-AQ through the NPC rather than indirect effects related to drug action or
199 activation.

200

201 Overall, these results suggest that the non-specific nature of the NPC renders the PVM
202 permeable to both metabolites important for parasite growth and several antimalarial drugs.
203 A comparison of the physicochemical properties of all molecules tested here suggests that
204 small water-soluble molecules reach the parasite via the NPCs. Hydrophobic or bulky
205 molecules cross the PVM independent of the NPCs (Table 1).

206

207 **NPCA influences susceptibility to PPQ**

208 PPQ, a 4-AQ used as partner drug in ART combination therapies, inhibits hemozoin formation
209 in the FV (Dhingra et al., 2017). In contrast to the other tested 4-AQ (Figures 2A-2C), EXP1^{low}
210 parasites became hypersensitive to PPQ (Figures 3A-3C). This unexpected finding suggested
211 that the mode of action of PPQ synergises with the phenotype of a reduced NPCA. It was
212 previously reported that besides inhibition of hemozoin formation PPQ also inhibits
213 hemoglobin proteolysis (Bopp et al., 2018; Dhingra et al., 2017; Sachanonta et al., 2011) which
214 may starve the parasites from hemoglobin derived-amino acids. Loss of EXP1 and
215 simultaneous inhibition of hemoglobin digestion may together aggravate the reduction of the
216 amino acid supply and render EXP1^{low} parasites more sensitive to PPQ. Supporting this
217 hypothesis, parasites treated with IC50⁹⁶ of PPQ became hypersensitive to amino acid
218 restriction (Figure 3D). Conversely, overexpression of EXP1 improved growth of PPQ-treated
219 parasites under amino acid restriction, suggesting that increased NPC levels restore amino
220 acid supply when hemoglobin digestion is inhibited (Figure 3D). In standard medium parasites
221 overexpressing EXP1 showed a trend for a decreased PPQ susceptibility compared to wt
222 parasites (Figures 3D and 3E). This may indicate that PPQ reaches the parasite independent

223 of the NPCs and that the elevated NPCA increased amino acid availability rather than PPQ
224 passage. These findings support the previously indicated dual mode of action of PPQ(Bopp et
225 al., 2018; Dhingra et al., 2017) and an important role of the NPCs in the acquisition of amino
226 acids from the host's serum when hemoglobin-derived amino acids are reduced.

227

228 **Reduced hemoglobin-derived amino acids cause fitness cost in ART^R parasites**

229 ART^R parasites display a fitness cost(Nair et al., 2018; Straimer et al., 2017) and ART^R field
230 isolates have a lower transition rate from ring to trophozoite stage when amino acid restricted
231 (Bunditvorapoom et al., 2018). As ART^R parasites show a reduced rate of endocytosis in ring
232 stages a shortened supply of amino acids from hemoglobin endocytosis may be a reason for
233 this fitness cost(Birnbaum et al., 2020). To test this idea, we first analysed the dependency of
234 ART^R parasites on amino acids from the culture medium which corresponds to the supply
235 parasites obtain from the host serum in natural infections. 3D7 parasites with a resistance-
236 conferring Kelch13 C580Y mutation (Kelch13^{C580Y})(Birnbaum et al., 2017) were more sensitive
237 to low amino acid levels than parasites with Kelch13wt (Figures 4A and 4B). This indicated
238 that ART^R parasites have an increased demand for amino acids when isogenic laboratory lines
239 are compared. This effect was specific for amino acids as these parasites behaved similarly to
240 controls under low glucose conditions or if growth was inhibited using NaN₃ (Figure 4A).

241

242 Isoleucine is the only amino acid absent from hemoglobin that the parasite needs to acquire
243 from the serum(Babbitt et al., 2012; Liu et al., 2006). To test whether the growth defect
244 observed in ART^R parasites is specific for a diminished supply of hemoglobin-derived amino
245 acids, we cultured sensitive and the 3D7 Kelch13^{C580Y} ART^R parasites in amino acid-restricted
246 medium with or without isoleucine. ART^R parasites showed a similar growth defect compared
247 to wild type parasites, irrespective of whether isoleucine was present or not (Figures 4C and
248 4D).

249

250 Phosphorylation of the eukaryotic initiation factor 2 α (eIF2 α) is a hallmark of the response to
251 amino acid starvation(Fennell et al., 2009). Previous studies showed increased eIF2 α
252 phosphorylation in ART^R parasites (Yang et al., 2019; Zhang et al., 2017) or when amino acids
253 were limiting(Babbitt et al., 2012; Fennell et al., 2009). To mimic amino acid deprivation in
254 the ring phase of ART^R parasites we cultured 3D7 rings under low amino acid conditions. These

255 parasites showed more phosphorylated eIF2 α than parasites grown in standard medium
256 (Figure 4E and S7C-S7D). Elevated levels of phosphorylated eIF2 α were also detected in ART^R
257 parasites grown in amino acid restricted medium. Supplementation with isoleucine alone did
258 not reduce the amount of phosphorylated eIF2 α , indicating that the reduced supply of
259 hemoglobin-derived amino acids in ring stages is sufficient to trigger an amino acid starvation
260 response. Altogether, these experiments support the idea that a shortage of hemoglobin-
261 derived amino acids is a cause for the fitness cost in ART^R parasites.

262

263 **EXP1 upregulation can compensate the fitness cost in ART^R parasites**

264 Previous work had indicated a role of EXP1 in ART resistance and *exp1* transcript levels were
265 observed to be upregulated in some resistant parasite lines (Lisewski et al., 2014; Rocamora
266 et al., 2018). Paradoxically, we here found that parasites with low NPCA had a decreased
267 susceptibility to DHA, indicative of a reduced passage of DHA molecules through the PVM
268 (Figures 2D, 2H and S2E-S2L). Thus, increased EXP1 levels would be expected to sensitise
269 parasites to ART rather than causing resistance. Indeed, overexpression of EXP1 increased the
270 susceptibility to ART (Figure 2G), although this likely is not clinically relevant at these ART
271 concentrations (Khoury et al., 2020) (see Supplementary Note 1). In agreement, we previously
272 found no evidence for a direct role of EXP1 in ART resistance (Mesen-Ramirez et al., 2019).
273 We therefore looked for alternative explanations for the elevated *exp1* mRNA levels reported
274 in ART^R parasites.

275

276 Since the NPCA is critical for amino acid acquisition, EXP1 levels might compensate the
277 reduced amino acid supply in ART^R parasites by increasing amino acid access via the NPCs. To
278 test this we overexpressed EXP1 (by an additional episomal copy of *exp1*) in the 3D7
279 Kelch13^{C580Y} parasites (Figures 4F and S4A) which reduced the growth defect under limiting
280 amino acid levels whereas no change was observed in low glucose medium or in the presence
281 of NaN₃ (Figures 4A and 4B). No difference was observed if EXP1 was overexpressed in
282 Kelch13wt parasites (Figures 4B and S4B). This indicated that specifically the amino acid
283 access through the NPC compensated for the endocytosis reduction in ART^R parasites.
284 Importantly, overexpression of EXP1 restored growth of ART^R parasites also in presence of
285 isoleucine (Figures 4C and 4D), connecting the effect to hemoglobin-derived amino acids.
286 These findings indicate that increased NPC levels compensate the fitness cost of ART

287 resistance by increasing the access to amino acids the parasite would otherwise obtain from
288 hemoglobin digestion. Overexpression of EXP2 (a protein also needed for NPC(Garten et al.,
289 2018)) in Kelch13^{C580Y} parasites did not significantly improve growth under low amino acid
290 conditions (Figures 4B and S4C), suggesting that its upregulation did not sufficiently raise the
291 NPCA to compensate the fitness cost in ART^R parasites.

292

293 As the resistant parasites used in these experiments had time to adapt to the fitness cost of
294 ART-resistance, we assessed the role of EXP1 in transgenic 3D7 parasites where endocytosis
295 can be conditionally reduced by partially inactivating Kelch13, leading to ART
296 resistance(Birnbaum et al., 2020). The experiments with these parasites (Kelch13-
297 3xNLS)(Birnbaum et al., 2017) confirmed the results with the Kelch13^{C580Y} parasites: after
298 partial inactivation of Kelch13, the parasites became hypersensitive to low amino acid but not
299 to low glucose levels or to growth inhibition by NaN₃. Under amino acid restriction growth of
300 parasites with an inactivated Kelch13 was improved two-fold when EXP1 was overexpressed
301 (+rap, 39.67%) compared to parasites with physiological levels of EXP1 (+rap, 19.37%) (Figures
302 4G and S4D).

303

304 Consistent with the findings in 3D7 parasites (Figures 2D, 2G and 2H), upregulation of EXP1
305 rendered Kelch13^{C580Y} parasites more sensitive to IC50^{96h} of DHA (Figure 4H; Supplementary
306 Note 1). Interestingly, Kelch13^{C580Y} parasites overexpressing EXP1 did not become more
307 sensitive to MFQ (Figure 4H). The reasons for this are unclear, but as also the response to
308 DHA was less than in 3D7, it is possible that resistance already resulted in compensatory
309 changes in these parasites.

310

311 **NPC upregulation is a natural mechanism to compensate amino acid restriction**

312 Our results indicated that elevated EXP1 levels can compensate the fitness cost in ART^R
313 parasites. To test if such a mechanism could be relevant in natural malaria infections, we
314 assessed *exp1* mRNA levels in blood samples of malaria patients with known ART resistance
315 characteristics(Zhu et al., 2021) from the TRACII study(van der Pluijm et al., 2020). Of these,
316 577 samples were analysed by microarray and 188 by RNA-Seq. Parasites in patients with
317 prolonged clearance times after ART treatment (indicative of ART resistance) had more *exp1*
318 transcripts than ART sensitive controls (Figures 5A and S5A-S5B). Estimation of parasite age

319 in the RNA-Seq samples(Lemieux et al., 2009; Zhu et al., 2018) indicated that this effect was
320 not due to a stage difference between the samples (Figure 5B). In addition, *exp1* mRNA levels
321 correlated positively with the level of resistance of the parasites in these samples (Figure 5C).
322 Ring stages of our 3D7 Kelch13^{C580Y} ART^R laboratory parasites also showed elevated *exp1*
323 mRNA levels compared to their isogenic control (Figure 5D and S6) whereas ART^R trophozoites
324 did not (Figure 5E).

325

326 To confirm these findings at the protein level we generated cell lines expressing endogenously
327 HA-tagged EXP1 in resistant (Kelch13^{C580Y}) and sensitive (Kelch13^{wt}) 3D7 parasites (Figures 5F
328 and S4E-S4F). ART^R rings (0-8 hpi) had higher EXP1 protein levels than Kelch13^{wt} parasites
329 (Figures 5G, 5H and S7E-S7F). ART^R trophozoites (24-32 hpi) also showed an increased amount
330 of EXP1 protein compared to sensitive parasites, presumably due to an accumulation of
331 protein from the entire ring phase. Overall these results indicated that in both, natural
332 infections and in laboratory lines, ART^R parasites compensated the reduced hemoglobin-
333 derived amino acid supply by increasing *exp1* transcription.

334

335 Next, we tested if parasites were capable to respond in a similar way when amino acid levels
336 were reduced in the medium. Both sensitive and ART^R parasites showed elevated *exp1* levels
337 in rings when selected under low amino acid conditions compared to parasites grown in
338 standard medium (Figure 5D), indicating that rings can adapt to low amino acid conditions by
339 increasing NPC levels. ART^R trophozoites did not further increase *exp1* transcripts in response
340 to amino acid deprivation, likely due to the baseline elevation of *exp1* transcripts in the
341 preceding ring, leading to sufficient accumulation of EXP1 protein in the PVM (Figures 5E and
342 5H). Transcript levels of *exp2* and several amino acid transporters (assumed to mediate amino
343 acid transport foremost at the parasite plasma membrane as known for ApiAT8(Blomqvist et
344 al., 2020)) were also increased in ART^R parasites and after selection in low amino acid medium
345 (Figure S6). While the transcript levels of amino acid transporters showed a mixed profile in
346 patient sample parasites, two were upregulated in parasites with a delayed clearance (Figure
347 S5). The ability of parasites to respond to low amino acid conditions by upregulating EXP1 was
348 also confirmed at the protein level. In parasites with an endogenously HA-tagged EXP1
349 (Figures S4E-S4G), EXP1 was elevated after growth under amino acid restriction for 4 weeks
350 compared to parasites grown in standard medium (Figures 5I, 5J and S7A-B).

351

352 Overall, these results show that ART^R parasites have elevated EXP1 levels and that parasites
353 respond in a similar way to growth in low amino acid medium. Since increasing EXP1 levels
354 mitigates the hypersensitivity of ART^R parasites to low amino acid conditions we propose that
355 EXP1-dependent upregulation of the NPCA is a natural mechanism in ART^R parasites to
356 increase the acquisition of amino acids from the host serum and to compensate the fitness
357 cost caused by their diminished hemoglobin endocytosis (Figure 6).

358

359

360 **Discussion**

361 Here we show that growth-relevant amounts of energy and carbon sources pass through the
362 PVM NPCs and that this activity is directly linked to the level of EXP1 activity. While the pore
363 size of the NPCs was already assessed electrophysiologically with dextrans and solutes in
364 freed parasites or isolated membranes(Desai et al., 1993; Desai and Rosenberg, 1997), our
365 growth assays show which molecules pass through the NPCs in living parasites and whether
366 this activity is relevant for parasite growth or not. Hypoxanthine and fatty acids were NPC-
367 independent, agreeing with the high passive membrane permeability of
368 hypoxanthine(Whittam, 1960) and the fact that fatty acids are not typically transported by
369 non-selective channels(Schwenk et al., 2010). The NPCs are already active in ring stages, as
370 previously postulated(Low et al., 2019; Mesen-Ramirez et al., 2019) and this may be the
371 reason for the delayed ring stage in Δ EXP1 parasites(Mesen-Ramirez et al., 2019).

372

373 It should be noted that the EXP1^{low} parasites still have partial NPCA and hence the observed
374 effect is smaller than the actual contribution of the NPCs to generate access for a particular
375 nutrient. However, as complete removal of *exp1* is lethal(Mesen-Ramirez et al., 2019), full
376 KOs are unsuitable for these experiments. While the standard RPMI medium contains an
377 excess of nutrients, the concentrations used in our limiting media are below those typical for
378 human serum(Brown and Guler, 2020; Kumar et al., 2020) (Supplementary Table 1). Such
379 conditions were previously used to show the importance for nutrient passage through the
380 RBC membrane which only becomes apparent if nutrients are limiting(Pillai et al., 2012).

381

382 Critically, we provide evidence that several antimalarial drugs pass through the NPCs. The
383 properties for NPC passage (Table 1) might inform medicinal chemistry approaches for lead
384 compounds with poor membrane permeability. While we found that modulation of NPC levels
385 alters drug access, this is constrained by the essential nutrient passage function. A diminished
386 NPCA is therefore unlikely to be an option for parasites to become resistant to drugs but the
387 NPCs may themselves represent a drug target that due to the broad functionality may not be
388 prone to resistance.

389

390 It was shown that non-ionised CQ passively passes into uninfected RBCs, indicating that this
391 may be the main mode of how CQ crosses membranes(Ferrari and Cutler, 1990, 1991).
392 However, only a very small fraction of all CQ molecules is in the non-ionised form at
393 physiological pH and evidence of ion-trapping in uninfected RBCs suggests that once in the
394 RBC, the proportion of ionised CQ may be even higher(Fitch et al., 1978; Macomber et al.,
395 1966). The predominance of this poorly membrane permeable ionised form of CQ could
396 explain our finding that CQ depends on the NPC to reach the parasite. This scenario likely
397 applies also for the other 4-AQ with the possible exception of PPQ for which the additional
398 mode of action precluded assessing NPC dependence with certainty in our assay. However,
399 as parasites do not become more sensitive to PPQ if EXP1 is overexpressed (in contrast to
400 MFQ), PPQ may be NPC-independent and this hypothesis fits with the larger molecular weight
401 and higher lipophilicity of PPQ compared to other 4-AQ (Table 1). Interestingly, Fluo-CQ, a
402 more hydrophobic analogue of CQ, did not to depend on the NPCs in both, our growth assay
403 and when microscopically monitoring uptake into the parasite. Hence, Fluo-CQ, as suggested
404 previously(Jida et al., 2017), has better passive membrane permeability but may be too bulky
405 for the NPC. As Fluo-CQ retains the mode of action of CQ(Jida et al., 2017), the findings with
406 this molecule show that our assay was not influenced by the mode of action of 4-AQ,
407 excluding such effects as a reason for the reduced susceptibility of EXP1^{low} parasites to 4-AQ.
408 Overall, our data therefore support the idea that 4-AQ, once in the RBC cytosol, do not
409 efficiently cross the PVM in a passive way but require the NPCs.

410

411 Our findings reveal a critical role for the parasite's amino acid supply in drug action and
412 resistance. ART^R parasites show diminished hemoglobin endocytosis in ring stages which is
413 expected to reduce amino acid levels(Birnbaum et al., 2020). The hypersensitivity of ART^R

414 parasites to low amino acid levels observed here as well as in previous work(Bunditvorapoom
415 et al., 2018) and the reversal of this effect by increasing the parasite's NPCA, lend
416 experimental evidence that amino acid deprivation contributes to the fitness cost in ART^R
417 parasites. Accordingly, we found evidence for elevated *exp1* mRNA levels in ART^R parasites
418 from human infections in South East Asia. Together with our *in vitro* work this indicates that
419 increased EXP1 levels, and possibly other means to increase amino acid acquisition, are a
420 compensatory mechanism of the parasite to reduce the fitness cost of ART resistance (Figure
421 6). Reducing either amino acid concentration in the medium, or Kelch13 levels (resulting in
422 ART resistance) or EXP1 levels, each prolong the ring stage(Birnbaum et al., 2020; Mesen-
423 Ramirez et al., 2019) and ART^R parasites also have a prolonged ring stage(Hott et al., 2015;
424 Mok et al., 2011), congruent with our conclusion that amino acid deprivation is an important
425 factor responsible for the fitness cost in ART^R parasites and that NPC levels influences this
426 factor. This fitness cost and the compensatory mechanisms in ART^R parasites are likely most
427 relevant in untreated hosts where Kelch13 wild-type parasites have a growth advantage over
428 ART^R parasites. In contrast, resistance itself is the deciding selection advantage over sensitive
429 parasites during the short times when the parasites are exposed to ART.

430
431 Our findings also support work indicating inhibition of hemoglobin proteolysis (thereby
432 reducing amino acid levels) as an additional mode of action for PPQ compared to that of other
433 4-AQ(Bopp et al., 2018; Dhingra et al., 2017). Hence, ART resistance and the frequently used
434 ART partner drug PPQ might pose a synergistic selection pressure to increase the amino acid
435 supply from sources other than hemoglobin and may have favoured compensatory changes
436 facilitating the development of resistance with this drug combination.

437
438 Distinguishing cause, effect and compensatory mechanisms in pathogen resistance is often
439 not straight forward. By modulating NPC levels and using restricted media this work indicates
440 an increased dependency on serum-derived amino acids as a downstream effect of ART
441 resistance and upregulation of EXP1 as a compensation mechanism, rather than being itself a
442 cause of resistance. Amino acids are critical for protein synthesis and have central functions
443 in cellular metabolism(Krishnan and Soldati-Favre, 2021). Isoleucine is the only amino acid
444 absent from hemoglobin. Reduced hemoglobin endocytosis in ART^R parasites is therefore not
445 expected to resemble isoleucine starvation(Babbitt et al., 2012). Nevertheless, the reduction

446 of hemoglobin-derived amino acids also resulted in a general amino acid deprivation response
447 as indicated by the eIF2 α phosphorylation. These results may explain the basal eIF2 α
448 phosphorylation in ART^R parasites(Yang et al., 2019; Zhang et al., 2017). However, the
449 deprivation of hemoglobin-derived amino acids will also result in effects specific to the
450 metabolic function of each kind of amino acid. For instance glutamine(Divo et al., 1985) is the
451 main carbon input of the mitochondrial TCA cycle in asexual blood stage parasites(MacRae et
452 al., 2013) and is known from other organisms to be required for the synthesis of many
453 metabolites, including glutathione and nucleotides(Krishnan and Soldati-Favre, 2021; Yoo et
454 al., 2020). The reduction of hemoglobin-derived amino acids indicated by our work could
455 therefore be one reason for some of the wide-ranging differences seen in ART^R parasites
456 compared to sensitive parasites(Mok et al., 2015; Mok et al., 2021; Sutherland et al., 2020;
457 Yang et al., 2019; Zhang et al., 2017).

458

459 It is possible that the trade-off between ART resistance and acquisition of amino acids limits
460 the extent of resistance achievable with the Kelch13-based resistance mechanism and
461 provides one possible explanation why full ART resistance has so far not arisen. In this
462 scenario the maximum capacity to obtain amino acids via the NPCs (and possibly other
463 components influencing amino acid levels in the parasite) limits the level of ART resistance,
464 because endocytosis cannot be further reduced without critically reducing amino acid levels
465 in the parasite (Figure 6). This also raises the prospect that host nutritional status, a factor
466 affecting the amino acid concentrations in the serum(Semba et al., 2016), may influence the
467 fitness cost of ART resistance and the efficacy of PPQ in *P. falciparum* infected individuals.
468 Knowing the factors incurring the fitness cost in ART^R parasites and the mechanisms of the
469 parasite to mitigate these effects could help identify further strategies that could contribute
470 to the current efforts to extend the usefulness of ART(Schallig et al., 2017; van der Pluijm et
471 al., 2020).

472

473 **SUPPLEMENTAL INFORMATION**

474 Supplemental information can be found online

475

476 **Acknowledgements**

477 We thank Ralf Krumkamp for help with statistical analysis and data presentation. This project
478 was funded by the German research foundation grant SP1209/4-1. M.E. and E.D.C. thank the
479 International Center for Frontier Research in Chemistry in Strasbourg and the Laboratoire
480 d'Excellence ParaFrap (grant LabEx ParaFrap ANR-11-LABX-0024 (E.D.C.)). Z.B. and Z.L.
481 acknowledge funding by the Singapore National Medical Research Council grant
482 #NMRC/OFIRG/0040/2017. α -EXP2 antibodies were obtained from The European Malaria
483 Reagent Repository (<http://www.malariaresearch.eu>). We thank Claudia Daubenberger for α -
484 GAPDH antibodies, Mike Blackman for Compound-2, Jacobus Pharmaceuticals for WR99210
485 and MR4/BEI Resources, NIAID, NIH for DSM1 (MRA-1161) and rabbit α -MSP1 (MRA-34).

486

487 **Author contributions**

488 P.M.R. and B.B. generated parasite lines, performed growth and uptake experiments and
489 analysed data with experimental contributions from C.C.P. H.vT. prepared RNA and
490 performed and A.B. supervised qRT-PCR analysis. M.E and E.D.C. synthesised fluorescent CQ
491 derivatives, provided reagents, physicochemical analysis of drugs and nutrients. Z.L and Z.B.
492 generated and analysed Microarray and RNA-Seq data from patient samples. P.M.R. and T.S.
493 conceived the study, supervised the project, designed experiments and interpreted results.
494 T.S., T.W.G., A.B., Z.B., and E.D.C. coordinated research. P.M.R. and T.S. wrote the original
495 manuscript and arranged figures. All authors reviewed and edited the final manuscript.

496

497 **Declaration of interests**

498 The authors declare no competing interests.

499

500 **Figure 1. NPC-dependence of nutrients**

501 (A) Rapalog-dependent generation of parasites relying on low levels of EXP1 (EXP1^{low}).

502 (B) Phenotypes of parasites relying on modified EXP1 versions. Left, EXP2 PVM distribution
503 (n=58 and n=80 from 2 independent experiments; *P* values, Fischer's exact test) and
504 immunofluorescence assay (IFA) images (middle) of trophozoites relying on EXP1 T_Mmut^{G83L}
505 (rapalog) compared to controls. Right, growth of these parasites (+rap) and controls (-rap) in
506 low amino acid versus complete medium. α -HA: endogenous EXP1-HA. DAPI, nuclei.

507 (C-D) Linear regression analysis of EXP2 distribution (C) or growth under low amino acids (D)
508 of parasites relying on the EXP1 constructs indicated in (B) or Figures S1A-G plotted against

509 activity of the construct (previously determined (Mesen-Ramirez et al., 2019) or in Figure S1J).
510 R^2 , coefficient of determination.

511 (E) Growth of $\text{cond}\Delta\text{EXP1}$ (-rap) and $\text{condEXP1}^{\text{low}}$ parasites ($\pm\text{rap}$) in low glucose versus
512 complete medium.

513 (F-G) Growth of EXP1^{low} (+rap) and control (-rap) parasites in low versus high hypoxanthine
514 (F) or lipid-free RPMI with low versus high oleic acid/palmitic acid (G). E, F and G, $n\geq 5$
515 biological replicates from ≥ 2 independent occasions.

516 (H) Live cell images of control and EXP1^{low} parasites (rapalog) after 2-NBDG uptake.

517 (I-J) Quantification of intracellular 2-NBDG fluorescence in EXP1^{low} or $\text{EXP1}^{\text{high}}$ (+rap)
518 trophozoites (I) or rings (J) compared to controls (-rap). EXP1^{low} , $n=91$ (-rap) and $n=80$ (+rap)
519 trophozoites from 3 and $n=64$ (-rap) and $n=57$ (+rap) rings from 2 independent experiments;
520 $\text{EXP1}^{\text{high}}$, $n=51$ (-rap) and $n=49$ (+rap) trophozoites from 2 and $n=88$ (-rap) and $n=92$ (+rap)
521 rings from 3 independent experiments. Mean, green line; P values, two-tailed unpaired t test
522 (B, E, F, G, I, J); Error bars, SD. (B, H), DIC, differential interference contrast; scale bars, 5 μm .

523

524 **Figure 2. NPC levels influence susceptibility to antimalarial drugs**

525 (A-G) Growth of control (-rap) and EXP1^{low} (+rap) parasites or 3D7 and EXP1 overexpressing
526 (3D7+EXP1) parasites exposed to $\text{IC}_{50}^{96\text{h}}$ of the drugs indicated versus growth without drug.

527 (H) Linear regression of growth after $\text{IC}_{50}^{96\text{h}}$ DHA exposure versus no DHA (see Figure S2E-
528 S2F) plotted as in Figure 1C and 1D.

529 (I) Growth of EXP1^{low} (+rap) and control parasites (-rap) exposed to lumefantrine $\text{IC}_{50}^{96\text{h}}$
530 versus no drug.

531 (J) Live cell images of Fluo-CQ uptake in $\text{condEXP1}^{\text{low}}$ parasites with low (rapalog) or control
532 levels of EXP1. DIC, differential interference contrast; scale bars, 5 μm .

533 (K) Quantification of Fluo-CQ fluorescence in the FV of parasites in (J). Mean (green line), $n=73$
534 (control) and $n=67$ (rapalog) parasites from 3 independent experiments.

535 (L) Growth of EXP1^{low} (+rap) and control parasites (-rap) exposed to Fluo-CQ $\text{IC}_{50}^{96\text{h}}$ versus
536 growth without Fluo-CQ. A-G, I and L, mean (green line) of ≥ 6 biological replicas from ≥ 2
537 occasions. Error bars, SD; P values, two-tailed unpaired t test.

538

539 **Figure 3. NPCA influences susceptibility to PPQ**

540 (A) Growth of control (-rap) and EXP1^{low} (+rap) parasites exposed to IC50^{96h} of PPQ versus
541 growth without PPQ.
542 (B) PPQ 96 h dose-response survival curve of control and EXP1^{low} (rapalog) parasites. Mean of
543 4 independent experiments.
544 (C) PPQ IC50⁹⁶ values from B. Mean, green line.
545 (D) Growth of 3D7 and EXP1 overexpressing (3D7+EXP1) parasites in complete (-) and amino-
546 acid limited medium (+low AA) exposed to IC50^{96h} of PPQ versus growth without PPQ.
547 (E) Growth of 3D7 and 3D7+EXP1 parasites with IC50^{96h} of PPQ versus growth without PPQ.
548 A, D, E, mean (green line) of ≥ 6 replicates from ≥ 3 independent experiments. Error bars, SD;
549 *P* values, two-tailed unpaired *t* test.

550

551 **Figure 4. Increased EXP1 levels compensate amino acid deficit in ART^R parasites**

552 (A-B) Growth of the indicated parasite lines under the indicated conditions (low AA, 1:20 AA)
553 compared to complete medium (high) or with or without sodium azide (NaN₃).
554 (C) Growth of the indicated parasites in amino acid-depleted (no AA) or limited medium (low
555 AA, 1:50 AA) versus growth in standard medium (high) \pm isoleucine (Ile).
556 (D) Growth of indicated parasites relative to 3D7 (red line) calculated from C. Points relative
557 to 3D7 in each experiment.
558 (E) Fold change of phosphorylated eIF2 α (P) in 3D7 and Kelch13^{C580Y} parasites grown in limited
559 medium (low AA, 1:50) \pm Ile versus standard medium (high AA, red line) quantified by
560 densitometry normalized to GAPDH. Blots in Figures S7C-S7D; n=3 independent experiments.
561 (F) IFA images of GFP-Kelch13^{C580Y} and GFP-Kelch13wt cell lines expressing EXP1-Ty^{high}. α -GFP,
562 endogenous Kelch13; α -Ty1, episomal EXP1-Ty1. Scale bars, 5 μ m.
563 (G-H) Growth of the indicated parasites in low AA versus growth in standard (G) or DHA or
564 MFQ (IC50⁹⁶) containing medium (H) versus growth without drug. (G) +rap, partial Kelch13
565 inactivation (Birnbaum et al., 2020). A-E and G-H, mean (green line); A-D and G-H $n \geq 6$
566 independent replicates. Error bars, SD; *P* values, two-tailed unpaired *t* test (B-D, G) or non-
567 parametric (Mann-Whitney) *t* test (A, G).

568

569 **Figure 5. EXP1 upregulation is a natural mechanism to compensate amino acid shortage**

570 (A) Violin plot of normalized *exp1* transcript levels in parasite samples from patients with the
571 indicated parasite clearance half-life (pch) after ART treatment. *P* values, one sided Mann-

572 Whitney test. Mean of n=81 samples with pch <5h (mean = -0.05855, non-resistant, blue) and
573 n=107 >5h (mean = 0.044324, resistant, red); h, hours.

574 (B) Raw *exp1* expression (log₂ ratio FKPM) versus estimated parasite age (hpi, hours post
575 invasion) in non-resistant (blue) and resistant (red) samples from (A).

576 (C) *exp1* expression vs pch after ART treatment of samples in (A).

577 (D-E) Left panels, *exp1* expression in rings (D) and trophozoites (E) quantified by qRT-PCR of
578 the indicated parasites grown in low and high AA medium and normalized to *aldolase*. Right
579 panel, fold change *exp1* expression under low AA versus high AA (red line). Mean (green line)
580 of n≥7 from 2 (rep1, rep2) (D) and 3 independent experiments (E).

581 (F) IFA images of GFP-Kelch13^{C580Y} (K13^{C580Y}) and GFP-Kelch13^{wt} (K13^{wt}) parasites with an HA-
582 tagged EXP1. α-GFP, Kelch13; α-HA, EXP1-HA. Scale bars, 5 μm.

583 (G) Immunoblot of stage specific parasite extracts of the cell lines shown in (F); α-GAPDH,
584 loading control.

585 (H) Fold change in EXP1-HA protein levels normalized to GAPDH in K13^{C580Y} versus K13^{wt}
586 parasites (red line) quantified from immunoblots in (G) and Figures S7E-S7F. Mean (green line)
587 of 3 independent experiments.

588 (I) Immunoblot of stage specific parasite extracts to detect endogenous EXP1-HA in parasites
589 grown under low AA (1:20) and high AA (standard RPMI). α-BIP, loading control. Asterisk,
590 unskipped EXP1-HA-NeoR (see Figure S4E).

591 (J) Fold change in EXP1 protein levels normalized to BIP in parasites under low AA versus high
592 AA (green line) quantified by densitometry from immunoblots in Figure S7A (4 independent
593 experiments).

594

595 **Figure 6. Model for amino acid supply in ART^R and sensitive parasites**

596 (A) *P. falciparum*-infected RBC showing sources of amino acids for the parasite.

597 (B) Changes in the balance of amino acid supply in ART^R and sensitive parasites.

598

599

600

601

602

603

604 **Table 1. Properties of substances tested**

Nutrient	MW (kDa)	H₂O solubility (g/L)	Charge[#]	NPC-dependence
Glucose	180.16	900 (soluble)	0	+
2-NBDG	342.26	10 (soluble)	0	+
Hypoxanthine	136.11	0.7 (insoluble)	0	-
Isoleucine	131.18	22.3 (soluble)	0	+
Oleic acid	282.47	1.5x10 ⁻⁵ (insoluble)	-	-
Palmitic acid	256.43	4x10 ⁻⁵ (insoluble)	-	-
Amodiaquine	355.87	47 (soluble)	++	+
Chloroquine	319.88	50 (soluble)	++	+
CQ1-NBD	540.02	soluble*	+	-
DHA	284.35	0.1 (insoluble)	0	+
Epoxomicin	554.37	insoluble*	0	-
Fluo-CQ	583.09	soluble*	+	-
Lumefantrine	528.94	>0.00005 (insoluble)	0	-
Mefloquine	378.32	1.8 (soluble)	+	+
MMV007839	312.19	n.t.	0	-
PPQ	535.52	13 (soluble)	+	-

605

606 *considered soluble or insoluble but no exact value available

607 #at pH=7

608 n.t.: not tested

609

610

611

612

613

614 **STAR Methods**

615

616 **RESOURCE AVAILABILITY**

617 **Lead contact**

618 Further information and requests for resources and reagents should be directed to and will

619 be fulfilled by the Lead Contact, Tobias Spielmann

620 spielmann@bni-hamburg.de

621

622 **Materials availability**

623 All unique reagents generated in this study can be obtained upon reasonable request to the

624 Lead Contact.

625

626 **Data and code availability**

627 **Examples**

628 The published article includes all data sets generated or analysed during this study.

629

630 **EXPERIMENTAL MODEL AND SUBJECT DETAILS**

631 ***Parasite cell lines***

632 Asexual intra-erythrocytic *P. falciparum* parasites (strain 3D7) were cultured in human
633 erythrocytes (O+) (transfusion blood, Universität Klinikum Eppendorf, Hamburg). Cultures
634 were grown in RPMI complete medium (Applichem, Darmstadt, Germany) containing 0.5%
635 Albumax (Invitrogen, Carlsbad, CA), 20 mM glucose and 200 mM hypoxanthine according to
636 standard procedures and maintained at 37°C in a microaerophilic atmosphere of 1% O₂, 5%
637 CO₂, and 94% N₂. Transgenic cell lines were maintained under drug selection with 2 µg/ml
638 Blasticidin S (Life Technologies) (for expression of the DiCre from pSkipFlox(Birnbaum et al.,
639 2017), 0.9 µM DSM1 (BEI Resources; <https://www.beiresources.org>) (for expression of EXP1
640 complementation constructs) and 400 µg/ml G418 (Sigma-Aldrich).

641

642 ***Human blood samples***

643 Samples from uncomplicated *P. falciparum* malaria patients were collected during a published
644 large epidemiological survey monitoring the spread of artemisinin resistance conducted
645 through the greater Mekong Sub regions (GMS) between 2016 and 2018. Information related
646 to age, sex, and gender identity (if known) of the subjects and sample size was already
647 provided (van der Pluijm et al., 2019; van der Pluijm et al., 2020). This survey was monitored
648 by the Mahidol-Oxford Tropical Medicine Research Unit Clinical Trials Support Group. Written
649 informed consent was obtained from all participants before the study was carried out and the
650 study protocol was approved by the Oxford Tropical Research Ethics Committee and for each
651 site by the appropriate institutional review board and/or the national ethics committee (van
652 der Pluijm et al., 2019; van der Pluijm et al., 2020). The study was registered
653 with [ClinicalTrials.gov](https://clinicaltrials.gov), number [NCT02453308](https://clinicaltrials.gov/ct2/show/study/NCT02453308).

654

655 **METHOD DETAILS**

656 **Cloning**

657 To generate EXP1-TMmut^{G83L}, a recodonised *exp1* gene(Mesen-Ramirez et al., 2019) was PCR
658 amplified with overlapping primers (see Supplementary Table 2 for all primers used in this
659 study) to introduce a single point mutation (G83L) in the transmembrane domain of EXP1 and
660 cloned into plasmid pEXP1comp containing the *nmd3* promoter(Mesen-Ramirez et al., 2019)
661 to drive the expression of EXP1-TMmut^{G83L} and γ DHODH as resistance marker.

662 To episomally express EXP1wt in the SLI-generated Kelch13 cell lines the recodonised *exp1*
663 gene(Mesen-Ramirez et al., 2019) was PCR amplified using primers to append the Ty1 epitope
664 tag sequence and cloned into the plasmid pEXP1comp(Mesen-Ramirez et al., 2019) using XhoI
665 and XmaI to place it under the control of the *hsp86* promoter. Next, the neomycin
666 phosphotransferase gene was PCR amplified from pSLI-2xFKBP(Birnbaum et al., 2017) and
667 used to exchange the γ DHODH resistance marker using BamHI and HindIII. This resulted in
668 pEXP1comp-NeoR. To episomally express EXP2-Ty1 in the SLI-generated Kelch13 cell lines a
669 recodonised *exp2* gene(Mesen-Ramirez et al., 2019) (GenScript) was PCR amplified and
670 cloned into pEXP1comp-NeoR using XhoI and AvrII.

671

672 To generate parasites expressing HA-tagged endogenous EXP1 via SLI(Birnbaum et al., 2017),
673 the last 467 bp of the *exp1* gene were amplified from 3D7 genomic DNA and cloned into pSLI-
674 HA(Mesen-Ramirez et al., 2016) using NotI and Sall to obtain pSLI-*exp1*-HA.

675

676 To modify the endogenous *exp1* locus in GFP-Kelch13^{wt} and GFP-Kelch13^{C580Y} parasites
677 (Birnbaum et al., 2017) (which are WR99210 and DSM1 resistant) via SLI, the last 467 bp of
678 the *exp1* gene were amplified with primers to append a triple HA tag. The neomycin
679 phosphotransferase gene was amplified with primers to append upstream a T2A skip peptide
680 (See Figure S4E). Both fragments were cloned into a vector containing blasticidine deaminase
681 as resistance marker(Mesen-Ramirez et al., 2016) using NotI and XmaI to generate a
682 promoterless plasmid (pSLI2-BSD).

683

684 **Parasite transfection**

685 For transfection of episomal constructs, mature schizonts were enriched with 60% Percoll and
686 resuspended in transfection buffer containing 50 μ g of plasmid DNA and electroporated using
687 a Nucleofector II (Lonza). For generation of complementation cell lines(Mesen-Ramirez et al.,
688 2019) cond Δ EXP1 parasites were transfected with pEXP1comp plasmids containing γ DHODH

689 as resistance marker and selection was done with 0.9 μ M DSM1 and BSD. Transgenic
690 Kelch13^{C580Y} and Kelch13+3NLS parasites(Birnbaum et al., 2017) were transfected with
691 pEXP1comp-Neo and pEXP2comp-Neo plasmids and selected with 400 μ g/ml G418 (Sigma-
692 Aldrich) to obtain Kelch13^{C580Y}+EXP1, Kelch13+3NLS+EXP1 and Kelch13^{C580Y}+EXP2.

693

694 **Preparation of nutrient-limited media**

695 To obtain amino acid-restricted RPMI medium, RPMI-1640 complete medium was added in a
696 1:20 dilution to amino acid-free RPMI medium 1640 (US Biological) containing 5% Albumax,
697 5 mM glucose and 200 μ M hypoxanthine. This resulted in a final concentration of 6 mM
698 glucose and 1:20 of the concentration of every amino acid found in standard RPMI complete
699 (Supplementary Table 1). For growth experiments in presence of isoleucine we adjusted the
700 amino acid restricted medium to a level that parasites would grow ~50% (compared to
701 standard medium) when isoleucine was added. For this RPMI-1640 complete medium was
702 added in a 1:50 dilution to amino acid-free RPMI and further supplemented with fresh
703 isoleucine to a final concentration of 382 μ M.

704

705 To prepare glucose-restricted medium, glucose-free RPMI medium (Gibco) containing 5%
706 Albumax and 200 μ M hypoxanthine was supplemented with D-(+) glucose monohydrate
707 (Merck) to a final concentration of 2.5 mM. For hypoxanthine-restricted medium RPMI
708 complete medium containing 5% Albumax was supplemented with hypoxanthine to a final
709 concentration of 500 nM. Lipid-free medium(Brancucci et al., 2017) was generated by
710 complementing RPMI-1640 complete (prepared as described above, without Albumax) with
711 0.39% fatty acid-free BSA (Sigma). To generate fatty acid- restricted medium oleic and
712 palmitic acids were added to this medium at a final concentration of 30 μ M each (Sigma-
713 Aldrich). Lyso PC (Avanti Polar Lipids) was added to this medium to a final concentration of
714 20 μ M from 30 mM ethanol-solved stocks as previously done(Brancucci et al., 2017). A second
715 medium containing 50 μ M of oleic and palmitic acids each was used as control medium
716 containing non-limiting amounts of fatty acids. Optimal nutrient concentrations to obtain a
717 parasite growth of ~50 % were determined experimentally (Figure S8H and S8I).

718

719 **Conditional EXP1 knock-out via DiCre-mediated excision in complementation cell lines**

720 Ring stages of *P. falciparum* transgenic and condEXP1 cell lines expressing Ty-tagged EXP1
721 with different modifications under different promoters (condEXP1^{low}, condEXP1^{mid} and
722 condEXP1^{high}) were synchronised twice with 5% sorbitol with a development stage window a
723 time window of 6 hours as described previously (Mesen-Ramirez et al., 2019). Parasite
724 cultures were divided into two culture dishes and rapalog (Clontech) was added to a final
725 concentration of 250 nM to one of the two dishes. The dish without rapalog served as control
726 culture. The medium was changed daily and the parasites further cultured in the presence of
727 rapalog for 48 hours. This resulted in EXP1^{low}, EXP1^{mid} and EXP1^{high} parasites (designated
728 'rapalog') that relied on the episomally expressed construct. These parasites were compared
729 to the matched controls that did not receive rapalog and still contained the genomic *exp1*
730 gene (designated 'control') and used for growth, uptake and immunofluorescence assays.

731

732 **Imaging**

733 Microscopy of live parasites and immunofluorescence assay was performed with a Zeiss
734 Axioscope M1 equipped with a 100X/1.4 numerical aperture oil immersion objective. A
735 Hamamatsu Orca C4742-95 camera and the Zeiss Axiovision software version 4.7 were used
736 for collecting images. Images were processed and overlaid with Corel PHOTO-PAINT X6
737 (<https://www.coreldraw.com>). Fluorescence quantifications were performed with Image J
738 version 1.46r (Schneider et al., 2012).

739

740 **Visualization of glucose, Fluo-CQ and CQ-NBD1 uptake**

741 Synchronised ring stages of EXP1^{low} (Δ EXP1 parasites relying on lowly expressed
742 complementing EXP1-Ty) or EXP1^{high} parasites (containing a highly expressed complementing
743 EXP1-Ty) obtained after one cycle with or without rapalog (see conditional diCre-based
744 excision of complemented knock-outs) were allowed to progress to trophozoites. For glucose
745 uptake, these trophozoites (24-30 hours post invasion) were washed once with RPMI medium
746 containing 1 mM glucose and then incubated in RPMI medium containing 1 mM glucose and
747 100 μ M 2-NBDG (Invitrogen) for 15 minutes at 37°C protected from light. The 2-NBDG stock
748 (10 mM in ethanol) was stored at -80°C and freshly diluted before each assay. For uptake in
749 ring stages, 4-12 hours post invasion rings were prepared similarly to the trophozoites but
750 cells were incubated for 2 hours at 37°C with 100 μ M 2-NBDG. For uptake of fluorescent CQ
751 analogues, trophozoites were washed twice with RPMI medium complete, followed by

752 incubation in RPMI medium containing 500 nM Fluo-CQ or 500 nM CQ1-NBD for 20 minutes
753 at 37°C protected from light. The DMSO-solved stock (5 mM) of each compound was stored
754 at -80°C and freshly diluted before each assay. After incubation of the parasites with 2-NBDG
755 or CQ analogues, the parasites were washed twice with RPMI medium containing 1 mM
756 glucose (glucose uptake) or RPMI complete (CQ uptake) and immediately imaged. All
757 micrographs were recorded blinded to the nature of the sample with the same acquisition
758 settings and exposure time. The fluorescence (as integrated density) in the parasite cytosol
759 and area of fluorescence in μm^2 were measured with Image J version 1.46r(Schneider et al.,
760 2012) and the background fluorescence was subtracted. For Fluo-CQ, the fluorescence in the
761 food vacuole (as integrated density) was measured. Images were processed with Corel
762 PHOTO-PAINT X6 (<https://www.coreldraw.com>) and the integrated density and the area
763 values were plotted using GraphPadPrism version 6.07.

764

765 **Flow cytometry (FC)**

766 Parasitemia of parasite cultures was determined as previously described using flow
767 cytometry(Birnbaum et al., 2017). For this, 20 μl resuspended parasite culture was incubated
768 in RPMI medium containing 4.5 $\mu\text{g}/\text{ml}$ dihydroethidium (Cayman Chemical) and 5 $\mu\text{g}/\text{ml}$
769 Hoechst (Cheomdex) for 20 minutes at room temperature protected from light. After this, the
770 cells were fixed with RPMI containing 0.003% glutaraldehyde. For every sample, 100,000
771 events were recorded using a LSRII flow cytometer (Beckton Dickinson), and the parasitemia
772 was determined with the FACS Diva Software. Gating strategy for infected RBCs is shown in
773 Figure S8J.

774

775 **Determination of 96 hours IC50 for antimalarial drugs and nutrients**

776 To determine the IC50 after two growth cycles for the drugs used in this study cond Δ EXP1
777 parasites were sorbitol synchronised and the start parasitemia was adjusted to approximately
778 0.1% in RPMI complete medium with 5% haematocrit. Equivalent volumes of cells were
779 cultured in 2 ml dishes containing RPMI complete with increasing concentrations of
780 chloroquine diphosphate (Sigma-Aldrich) [0-100 nM], mefloquine (MFQ) hydrochloride
781 (Sigma-Aldrich) [0-250 nM], DHA (Adipogen) [0-10 nM], amodiaquine (Santa Cruz
782 Biotechnology) [0-50 nM], lumefantrine (Sigma-Aldrich) [0-250 nM], piperazine
783 tetraphosphate tetrahydrate (Sigma-Aldrich) [0-50 nM], MVV007839 (Medicines for Malaria

784 Ventures (www.mmv.org), kindly provided by Eric Beitz, Christian-Albrechts-Universität, Kiel)
785 [0-500 nM], epoxomicin (Sigma-Aldrich) [0-100 nM], Fluo-CQ(Jida et al., 2017) and CQ1-NBD
786 [0-50 nM]. For determination of the concentration when nutrient concentration limited
787 growth to 50% after 96h ('IC50^{96h}' of nutrients), the parasite cells were cultured with
788 increasing concentrations of hypoxanthine [0-4000 µM] (Sigma-Aldrich) added to
789 hypoxanthine free medium, oleic acid/palmitic acid [0-70 µM] (Sigma-Aldrich) added to lipid
790 free medium and glucose [0-50 mM] added to medium without glucose. Before culturing in
791 these media, the parasites were first washed twice with the corresponding nutrient-depleted
792 medium (for nutrient-free media see preparation of nutrient-limited media). The curves for
793 determination of IC50⁹⁶ are shown in Figure S2A-S2D and S8A-S8G.

794
795 To compare IC50 values of DHA and MFQ between parasites expressing physiological levels
796 of EXP1 and EXP1^{low} parasites, synchronous ring stages of EXP1wt^{low} parasites (i.e. after
797 rapalog-mediated excision of the genomic *exp1*, see conditional EXP1 knock-out via DiCre-
798 mediated excision in complementation cell lines) and the matched controls grown without
799 rapalog were diluted to 1% (rapalog) and 0.1 % (control parasites) parasitemia in RPMI
800 complete medium. Equivalent volumes of cells were cultured with RPMI complete medium
801 containing increasing concentrations of MFQ hydrochloride (Sigma-Aldrich) [0-300 nM] and
802 DHA (Adipogen) [0-10 nM] and the selection drugs to maintain the genetic alterations and the
803 episomal plasmid of the used cell lines. The start parasitemia was determined by FC and the
804 medium of the cultures changed daily for four days (thereby adding fresh drug every day).
805 The final parasitemia for every drug concentration was measured at day five by FC and the
806 start parasitemia was subtracted from the final parasitemia to obtain the adjusted final
807 parasitemia. The IC50 values were calculated using GraphPadPrism version 6.07.

808

809 **Growth assays under nutrient limiting conditions and in presence of drug at IC50^{96h}**

810 To evaluate growth under low nutrient conditions, EXP1wt^{low}, EXP1wt^{mid} and EXP1wt^{high} ring
811 stage parasites (i.e. after excision of the endogenous genes from the condΔEXP1 parasites in
812 the previous cycle to obtain parasites relying on the complementing constructs) and the
813 matched controls grown without rapalog (see conditional EXP1 knock-out via DiCre-mediated
814 excision in complementation cell lines) were diluted in RPMI complete and the parasitemia
815 was adjusted to 0.1% (control) and 0.5% (rapalog), respectively. The cultures were washed

816 twice with the corresponding RPMI nutrient-restricted medium (glucose, amino acid,
817 hypoxanthine or lipid-free medium). Equivalent volumes of the washed cells were transferred
818 to 2 ml dishes containing either RPMI complete medium or the corresponding nutrient-
819 restricted medium. For drug susceptibility, the cells were transferred to RPMI complete
820 without drugs or RPMI containing the IC₅₀^{96h} determined for each drug: 15 nM chloroquine
821 diphosphate, 7 nM MFQ hydrochloride (diluted from a 48.3 mM DMSO-solved stock), 2.5 nM
822 amodiaquine, 1nM DHA (diluted from a 250 μM DMSO-solved stock), 33 nM lumefantrine
823 (diluted from a 5 mM DMSO solved stock), 3 nM piperazine tetraphosphate tetrahydrate
824 (diluted from a water-solved 5.25 mM stock), 160 nM MVV007839, 2.5 nM epoxomicin
825 (diluted from a 180 μM DMSO-solved stock), 10 nM Fluo-CQ and 8 nM CQ1-NBD, diluted from
826 a 5 mM DMSO-solved stock). The curves for determination of IC₅₀⁹⁶ are shown in Figure S2A-
827 S2D and S8A-S8I.

828

829 For determination of susceptibility to low amino acid conditions, 3D7 wild type, 3D7+EXP1
830 and the transgenic Kelch13 cell lines (Kelch13^{C580Y}, Kelch13^{C580Y}+EXP1, Kelch13^{C580Y}+EXP2,
831 Kelch13+3xNLS and Kelch13+3xNLS+EXP1) were synchronised twice with 5% sorbitol to
832 obtain a development stage window of 5 hours. Ring stages of the next cycle were diluted to
833 0.1% parasitemia in complete RPMI medium and washed twice with RPMI low AA or with
834 RPMI low glucose (depending on the nutrient assayed). Equal volumes of these cells were
835 transferred to 2 ml dishes with RPMI complete with and without rapalog (250 nM), RPMI
836 without AA, RPMI without AA ± 382 μM isoleucine, RPMI low AA (1:50) ± 382 μM isoleucine,
837 low AA (1:20) ± rapalog, RPMI low glucose ± rapalog and RPMI complete containing 75 μM
838 NaN₃ (Sigma-Aldrich) ± rapalog. Cultures were fed daily with fresh medium containing the
839 drugs to maintain the genetic modifications of the respective cell lines. For induction of knock
840 sideways in Kelch13+3xNLS cell lines, fresh rapalog was added each day and parasites were
841 maintained in the corresponding medium in presence or absence of rapalog for two growth
842 cycles.

843

844 Initial (day 0) and final parasitemia (day 5) were measured using FC and initial parasitemia
845 was subtracted from the final parasitemia to obtain the adjusted final parasitemia. Relative
846 growth for each cell line and condition was calculated as the adjusted final parasitemia in

847 restricted medium or medium containing IC50⁹⁶ of each drug versus the adjusted final
848 parasitemia in RPMI complete medium without drug.

849

850 **Immunofluorescence assays**

851 To assess localization of EXP2 in the EXP1 complementation cell lines, the parasites were
852 prepared for IFA as follows: ring stage parasites relying on the complementing constructs (i.e.
853 after excision of the endogenous genes from the condΔEXP1 parasites in the previous cycle,
854 see conditional EXP1 knock-out via DiCre-mediated excision in complementation cell lines)
855 and the matched controls grown without rapalog were sorbitol synchronised and allowed to
856 develop to 24-30 h.p.i trophozoites. Thereafter the cells were washed once in 1x PBS and
857 fixed with 4% paraformaldehyde/0.0075% glutaraldehyde as described (Mesen-Ramirez et al.,
858 2019; Tonkin et al., 2004) and used for IFA with the cells in suspension.

859 To evaluate the localization of the Ty-tagged EXP1-TMmut^{G83L} complementation construct
860 the cells were prepared for IFA as follows to distinguish protein localized at the PPM from
861 that localized at the PVM as previously established (Mesen-Ramirez et al., 2019): Compound
862 2 (Taylor et al., 2010) (a kind gift of Mike Blackman, the Francis Crick Institute, London) was
863 added to trophozoite stages at 1 μM final concentration and grown overnight to obtain
864 arrested-schizonts that were fixed in 4% paraformaldehyde/0.0075% glutaraldehyde as
865 described (Mesen-Ramirez et al., 2019; Tonkin et al., 2004) and used for IFA with cells in
866 suspension.

867 The IFA with the fixed cells was carried out essentially as described (Mesen-Ramirez et al.,
868 2019; Tonkin et al., 2004). The cells were permeabilised with 0.5% Triton X-100 in PBS,
869 blocked with 3% BSA in PBS and incubated in suspension for 1 hour with primary antibodies:
870 rabbit α-HA (Cell Signaling Technology) (1:500), mouse α-Ty (Sigma) (1:20,000) and rabbit α-
871 MSP1 (PPM marker [1:1,000]) (MRA-34, BEI Resources; <https://www.beiresources.org>) and
872 mouse monoclonal 7.7 α-EXP2 (European Malaria Reagent Repository
873 (<http://www.malariaresearch.eu>) (1:2,000) diluted in 3% BSA in PBS. After incubation with
874 the primary antibody the cells were washed three times with PBS with intermittent
875 centrifugations at 16,000g to change solutions and further incubated for 1 hour with Alexa
876 Fluor 488 or Alexa Fluor 594 conjugated secondary antibodies specific for mouse and rabbit

877 IgG (Invitrogen) diluted 1:2,000 in 3% BSA in PBS and containing 1 µg/ml DAPI. Before imaging
878 cells were washed five times with PBS.

879 To quantify the percentage of cells with a correct or aberrant localization of EXP2 at the PVM,
880 parasites were counted (operator blinded to the identity of the sample) and classified as
881 correct when EXP2 exhibited more than 50 % circumferential localization of the signal and as
882 aberrant when less than 50% of the cell was surrounded by fluorescence.

883 For localization of EXP1-Ty in Kelch13 and 3D7 cell lines asynchronous parasite cultures were
884 harvested, washed twice with PBS, air-dried as thin monolayers on 10-well slides (Thermo
885 Fischer) and fixed in 100% acetone for 30 minutes at room temperature as described (Mesen-
886 Ramirez et al., 2019; Spielmann et al., 2003). After rehydration with PBS, the cells were
887 labelled with mouse α-Ty (Sigma) (1:20,000) and α-GFP rabbit (Thermo Fischer) (1:500) for
888 detection of GFP-tagged endogenous Kelch13wt and Kelch13^{C580Y}. Washes and incubation
889 with secondary antibodies was performed as described above but carried out on the slide that
890 was kept in a humid chamber. Slides were sealed with a cover slip using mounting medium
891 (Dako).

892

893 **Total protein extracts**

894 For detection of EXP1wt-Ty1 in total parasite extracts of Kelch13 cell lines, an asynchronous
895 culture was incubated with 0.03% saponin in PBS for 10 minutes on ice to lyse the host cells
896 of the parasites and uninfected RBCs (saponin pellets). After three washes with DPBS proteins
897 were extracted from the parasite pellet with protein lysis buffer (0.5x PBS/4% SDS/0.5% Triton
898 X-100) containing protease cocktail inhibitor (Roche) and 1mM PMSF. After centrifugation at
899 16,000g for 5 minutes, the supernatant was transferred to a fresh tube and pellet and
900 equivalent amounts of the supernatant were diluted with reducing SDS sample buffer and
901 analysed by SDS-PAGE immunoblotting.

902

903 **Solubility assays**

904 To distinguish PV soluble proteins from parasite-internal and membrane-associated proteins,
905 trophozoites of EXP1-TMmut^{G83L}-Ty1 (from 5 ml culture with a parasitemia of ~5%) were
906 enriched in a Percoll gradient (Heiber et al., 2013), washed twice with PBS and incubated on

907 ice for 10 minutes with 100 μ l PBS containing 0.015% saponin (Sigma) and centrifuged at
908 16,000g for 5 minutes. The supernatant (PV and host cell soluble proteins) was transferred to
909 a new tube and mixed with protease cocktail inhibitor (Roche), 1 mM PMSF and reducing SDS
910 sample buffer. The parasite pellet (membrane proteins and soluble proteins within the
911 parasite) was resuspended in 100 μ l of protein lysis buffer containing complete protease
912 inhibitor cocktail and 1 mM PMSF. The pellet lysate was cleared by centrifugation at 16,000g
913 for 5 minutes, transferred to a new tube and mixed with reducing SDS sample buffer.
914 Equivalent volumes of the pellet lysate and the supernatant containing the soluble proteins
915 were analyzed by SDS-polyacrylamide gel electrophoresis (PAGE) and immunoblotting.

916

917 **Immunoblotting**

918 Protein samples separated by SDS-PAGE were transferred to Amersham Protran membranes
919 (GE Healthcare, Germany) in a tankblot device (Bio-Rad) using transfer buffer (0.192 M
920 glycine, 0.1% SDS, 25 mM Tris-HCl pH=8.0) with 20% methanol. Membranes were blocked for
921 30 minutes with PBS containing 5% skim milk. Primary antibodies were diluted in PBS
922 containing 5% skim milk and incubated with membranes overnight in the following dilutions:
923 mouse α -Ty (Sigma), 1:20,000; mouse α -GFP (Roche), 1:1000; rabbit α -SBP1(C)(Mesen-
924 Ramirez et al., 2016), 1:2,000; rabbit anti-BIP(Struck et al., 2005), 1:2,000; rabbit anti-phospho
925 eIF2 α (Ser51) (Cell Signaling), 1:1000 and mouse anti-GAPDH (Daubengerger et al., 2000),
926 1:2000. After three washes with PBS, horseradish peroxidase-conjugated secondary
927 antibodies goat α -mouse (Dianova), 1:3,000 or donkey α -rabbit (Dianova), 1:2,500 were
928 added to the membrane in PBS containing 5% skim milk and incubated for 2 hours. Detection
929 was done after three washes with PBS using enhanced chemiluminescence (Bio-Rad/Thermo
930 Fischer), and signals were recorded with a ChemiDoc XRS imaging system (Bio-Rad).

931

932 **Quantitative reverse transcription real-time PCR**

933 Kelch13wt-GFP and Kelch13^{C580Y}-GFP(Birnbaum et al., 2017) parasites were cultured in
934 parallel in RPMI complete and amino acid restricted medium for 4 months (~60 development
935 cycles). Tightly synchronised 4-12 h.p.i old rings and 24-32 h.p.i old trophozoites were
936 harvested and centrifuged at 2000 r.p.m for 5 minutes. The cell pellets were thoroughly
937 resuspended in five volumes TRIzol (Life Technologies), incubated for 5 minutes at 37°C and
938 stored at -80°C until RNA purification. RNeasy Mini (Qiagen) with on-column DNase I (Qiagen)

939 treatment was used for RNA purification. Absence of gDNA was checked for each sample
940 using 50 ng RNA and the *sbp1* primer set. If necessary, DNasing was repeated until the sample
941 was free of any DNA contamination by qPCR. Afterwards, cDNA was synthesized with the
942 SuperScript III Reverse Transcriptase (Invitrogen) primed with random hexamers (Invitrogen)
943 at 50°C for 1 hour.

944

945 The LightCycler 480 (Roche) was used for quantitative real-time PCR analysis using the
946 provided software version 1.5. cDNA template was mixed with QuantiTect SYBR Green PCR
947 reagent (Qiagen) and 0.3 µM sense and antisense primer in a final volume of 10 µl. Reactions
948 were incubated at 95°C for 15 minutes, then subjected to 40 cycles of 95°C for 15 seconds
949 and 60°C for 1 minute and a subsequent melting step (60–95°C). The specificity of each primer
950 pair was confirmed after each RT-qPCR run by dissociation curve analysis. Ct calculation was
951 done using the fit points analysis method provided by the software. Relative quantification of
952 *exp1* and *exp2* expression levels normalized to the expression of *fructose-bisphosphate*
953 *aldolase* (PF3D7_1444800) was performed using primer sets described in Supplementary
954 Table 2. To control for slight stage differences between the different cell lines, primer pairs
955 targeting the putative *mitochondrial import receptor subunit tom22* (PF3D7_0524700), the *T-*
956 *complex protein 1 subunit theta* (PF3D7_0214000), *early transcribed membrane protein 5*
957 (*etramp5*, PF3D7_0532100), *apical membrane antigen 1* (*ama1*, PF3D7_1133400) as well as
958 the housekeeping gene *arginyl-tRNA synthetase* (PF3D7_1218600) were included
959 (Supplementary Table 2). Relative expression data (RELATEXP) were corrected for
960 amplification efficiency of each primer pair, which was determined by dilution of a single
961 cDNA from 3D7 over 5–6 logs of concentration (Supplementary Table 2).

962

963 **Transcriptional profiling of *P. falciparum* parasites from patient blood**

964 Samples from uncomplicated *P. falciparum* malaria patients had previously been collected
965 during a published large epidemiological survey monitoring the spread of artemisinin
966 resistance conducted throughout the greater Mekong Sub regions (GMS) between 2016 and
967 2018 (van der Pluijm et al., 2020). This survey was monitored by the Mahidol-Oxford Tropical
968 Medicine Research Unit Clinical Trials Support Group, had written informed consent from all
969 participants before the study was carried out and the study protocol was approved by the

970 Oxford Tropical Research Ethics Committee and for each site by the appropriate institutional
971 review board and/or the national ethics committee(van der Pluijm et al., 2020). The mRNA
972 profiling was conducted with total RNA extracted from the parasitized blood samples
973 collected from the patients using DNA microarrays and Next generation Sequencing (RNA-
974 Seq) as described(Kucharski et al., 2020). Data analysis for the Transcriptome-Wide
975 Association Studies of artemisinin resistance encompassing the entire dataset is currently
976 under preparation (Zhu et al., 2021)

977

978 **Developmental stage estimation of field samples**

979 The method of age estimation for the field parasite samples was described
980 previously(Lemieux et al., 2009; Zhu et al., 2018). In brief, it was determined by a mixture
981 linear regression model presented in the following formula:

$$982 \quad E_g = (1-\alpha)*x_g(hr) + \alpha*z_g + \varepsilon_g \quad ,$$

983 Where E_g is a gene's expression value in a parasite field sample, $x_g(hr)$ is that gene's reference
984 expression level at the asexual stage of hpi hr , z_g denote the average reference expression of
985 sexual stages (from the 5th to 12th day during gametocytes developing), α is the proportion of
986 gametocytes to the total parasite count (sum of sexual and asexual parasites) and ε_g is the
987 associated error term. The reference asexual transcriptomes were generated during asexual
988 intraerythrocytic cycle in *P. falciparum* 3D7 strain with two hours intervals of 48 hours (GEO
989 accession number GSE149865). The reference gametocyte transcriptomes are accessible via
990 GEO accession number GSE121505. The result was obtained based on the maximum log-
991 likelihood values evaluated over a grid of mixtures for varying the gametocyte proportion α ,
992 and hpi hr , for each sample. The details are available in the paper under review (Zhu et al.,
993 2021).

994

995 **Time resolved expression of EXP1 under low amino acid conditions**

996 To analyse differences in protein levels of EXP1 parasites expressing endogenous tagged
997 EXP1-HA were cultured four weeks in RPMI low AA and RPMI complete. Percoll-purified
998 schizonts of every condition were allowed to invade fresh RBCs with shaking for 30 minutes
999 at 37°C and cultured for eight hours under standard conditions. 0-8 hours post invasion (h.p.i)
1000 old ring stages were sorbitol synchronised and washed twice with the corresponding RPMI

1001 medium. Cell pellet was divided into 4 dishes and hematocrit adjusted to 5%. One dish
1002 corresponding to the first time point (0-8 h.p.i) was incubated with DPBS containing 0.03%
1003 saponin and proteins were extracted from the parasite pellet with protein lysis buffer (0.5x
1004 PBS/4% SDS/0.5% Triton X-100) as described above for total protein extracts. The remaining
1005 dishes were further cultured under standard conditions with the corresponding medium,
1006 harvested sequentially every eight hours to obtain the time points 8-16, 16-24 and 24-32 h.p.i.
1007 and lysed as described above. Samples were stored at -20 °C until all samples were collected
1008 and analysed in parallel by immunoblotting. For densitometric analysis, detection was done
1009 by enhanced chemiluminescence (Bio-Rad/Thermo Fischer) and signals were recorded with a
1010 ChemiDoc XRS imaging system (Bio-Rad). Intensity of HA signal of EXP1-HA and BIP for every
1011 time point was quantified with Image Lab software 5.2 (Bio-Rad). HA signal was normalized
1012 to the BIP signal and the ratio under low AA was compared to that under complete, which
1013 was set to 100%.

1014

1015 **Detection of eIF2 α phosphorylation**

1016 Schizont stages of 3D7 and Kelch13^{C580Y}-GFP parasites were Percoll purified and allowed to
1017 invade fresh RBCs with shaking for 30 minutes at 37°C, cultured for three hours in standard
1018 medium and in RPMI low AA (1:50) \pm 382 μ M isoleucine. The 0-3 h.p.i old ring stages were
1019 sorbitol synchronised and washed twice with the corresponding media. Ring stages were
1020 further cultured for five hours in the corresponding media and saponin pellets were prepared
1021 from 5-8 h.p.i old ring stages. Samples were analysed by Western Blot to detect
1022 phosphorylated eIF2 α and GAPDH.

1023

1024

1025

1026 **QUANTIFICATION AND STATISTICAL ANALYSIS**

1027 Unless otherwise indicated, statistical significance was calculated using a two-tailed unpaired
1028 t-test performed using GraphPad Prism v6.07. Statistical parameters for each experiment
1029 including means, regression coefficients and n values are provided in figure legends. Error
1030 bars denote standard deviation. n indicated individual parasite cells, biological replicates or
1031 independent experiments. Significance was defined from the calculated *P* values where *P* >
1032 0.05 corresponds to a not significant difference.

1033

1034 No power analysis was performed. For growth assays at least three independent experiments
1035 were performed separately in different days or by different analysts and for phenotypical
1036 analysis (distribution of EXP2, uptake of 2-NBDG and CQ fluorescent analogues) at least three
1037 independent experiments were performed in different days for each condition with $n \geq 20$
1038 individual cells per experiment.

1039

1040 For phenotypical analyses and growth assays, samples were allocated into two groups -
1041 rapalog (control) and + rapalog to induce EXP1 KO. If drugs were added control culture \pm
1042 rapalog under standard physiological conditions was analysed side by side. For growth assays
1043 under nutrient-restricted conditions cell lines were grown in parallel under standard
1044 physiological conditions. For microscopical analyses, image acquisition was performed from
1045 random fields containing infected RBCs based on the DIC or DAPI channel. For microscopical
1046 scoring the identity of samples (\pm rapalog) were blinded to the analyst (EXP2 distribution;
1047 uptake of 2-NBDG and CQ fluorescent analogues). Due to the obvious differences in the
1048 phenotype of cells, blinding was not always effective.

1049

1050 **References**

- 1051 Amaratunga, C., Sreng, S., Suon, S., Phelps, E.S., Stepniewska, K., Lim, P., Zhou, C., Mao, S., Anderson,
1052 J.M., Lindegardh, N., *et al.* (2012). Artemisinin-resistant *Plasmodium falciparum* in Pursat province,
1053 western Cambodia: a parasite clearance rate study. *Lancet Infect Dis* *12*, 851-858.
- 1054 Arieu, F., Witkowski, B., Amaratunga, C., Beghain, J., Langlois, A.C., Khim, N., Kim, S., Duru, V., Bouchier,
1055 C., Ma, L., *et al.* (2014). A molecular marker of artemisinin-resistant *Plasmodium falciparum* malaria.
1056 *Nature* *505*, 50-55.
- 1057 Asahi, H., Kanazawa, T., Kajihara, Y., Takahashi, K., and Takahashi, T. (1996). Hypoxanthine: a low
1058 molecular weight factor essential for growth of erythrocytic *Plasmodium falciparum* in a serum-free
1059 medium. *Parasitology* *113 (Pt 1)*, 19-23.
- 1060 Babbitt, S.E., Altenhofen, L., Cobbold, S.A., Istvan, E.S., Fennell, C., Doerig, C., Llinas, M., and Goldberg,
1061 D.E. (2012). *Plasmodium falciparum* responds to amino acid starvation by entering into a hibernatory
1062 state. *Proc Natl Acad Sci U S A* *109*, E3278-3287.
- 1063 Birnbaum, J., Flemming, S., Reichard, N., Soares, A.B., Mesen-Ramirez, P., Jonscher, E., Bergmann, B.,
1064 and Spielmann, T. (2017). A genetic system to study *Plasmodium falciparum* protein function. *Nat*
1065 *Methods* *14*, 450-456.
- 1066 Birnbaum, J., Scharf, S., Schmidt, S., Jonscher, E., Hoeijmakers, W.A.M., Flemming, S., Toenhake, C.G.,
1067 Schmitt, M., Sabitzki, R., Bergmann, B., *et al.* (2020). A Kelch13-defined endocytosis pathway mediates
1068 artemisinin resistance in malaria parasites. *Science* *367*, 51-59.
- 1069 Blomqvist, K., Helmelt, M., Wang, C., Absalon, S., Labunska, T., Rudlaff, R.M., Adapa, S., Jiang, R., Steen,
1070 H., and Dvorin, J.D. (2020). Influence of *Plasmodium falciparum* Calcium-Dependent Protein Kinase 5
1071 (PfCDPK5) on the Late Schizont Stage Phosphoproteome. *mSphere* *5*.

1072 Bopp, S., Magistrado, P., Wong, W., Schaffner, S.F., Mukherjee, A., Lim, P., Dhorda, M., Amaratunga,
1073 C., Woodrow, C.J., Ashley, E.A., *et al.* (2018). Plasmepsin II-III copy number accounts for bimodal
1074 piperazine resistance among Cambodian *Plasmodium falciparum*. *Nat Commun* *9*, 1769.

1075 Brancucci, N.M.B., Gerdt, J.P., Wang, C., De Niz, M., Philip, N., Adapa, S.R., Zhang, M., Hitz, E.,
1076 Niederwieser, I., Boltryk, S.D., *et al.* (2017). Lysophosphatidylcholine Regulates Sexual Stage
1077 Differentiation in the Human Malaria Parasite *Plasmodium falciparum*. *Cell* *171*, 1532-1544 e1515.

1078 Brown, A.C., and Guler, J.L. (2020). From Circulation to Cultivation: *Plasmodium* In Vivo versus In Vitro.
1079 *Trends Parasitol* *36*, 914-926.

1080 Bunditvorapoom, D., Kochakarn, T., Kotanan, N., Modchang, C., Kumpornsin, K., Loesbanluechai, D.,
1081 Krasae, T., Cui, L., Chotivanich, K., White, N.J., *et al.* (2018). Fitness Loss under Amino Acid Starvation
1082 in Artemisinin-Resistant *Plasmodium falciparum* Isolates from Cambodia. *Sci Rep* *8*, 12622.

1083 Combrinck, J.M., Mabothe, T.E., Ncokazi, K.K., Ambele, M.A., Taylor, D., Smith, P.J., Hoppe, H.C., and
1084 Egan, T.J. (2013). Insights into the role of heme in the mechanism of action of antimalarials. *ACS Chem*
1085 *Biol* *8*, 133-137.

1086 Cowell, A.N., and Winzeler, E.A. (2019). The genomic architecture of antimalarial drug resistance. *Brief*
1087 *Funct Genomics* *18*, 314-328.

1088 Cowman, A.F., Galatis, D., and Thompson, J.K. (1994). Selection for mefloquine resistance in
1089 *Plasmodium falciparum* is linked to amplification of the *pfmdr1* gene and cross-resistance to
1090 halofantrine and quinine. *Proc Natl Acad Sci U S A* *91*, 1143-1147.

1091 Daubenberger, C.A., Poltl-Frank, F., Jiang, G., Lipp, J., Certa, U., and Pluschke, G. (2000). Identification
1092 and recombinant expression of glyceraldehyde-3-phosphate dehydrogenase of *Plasmodium*
1093 *falciparum*. *Gene* *246*, 255-264.

1094 Desai, S.A., Bezrukov, S.M., and Zimmerberg, J. (2000). A voltage-dependent channel involved in
1095 nutrient uptake by red blood cells infected with the malaria parasite. *Nature* *406*, 1001-1005.

1096 Desai, S.A., Krogstad, D.J., and McCleskey, E.W. (1993). A nutrient-permeable channel on the
1097 intraerythrocytic malaria parasite. *Nature* *362*, 643-646.

1098 Desai, S.A., and Rosenberg, R.L. (1997). Pore size of the malaria parasite's nutrient channel. *Proc Natl*
1099 *Acad Sci U S A* *94*, 2045-2049.

1100 Dhingra, S.K., Redhi, D., Combrinck, J.M., Yeo, T., Okombo, J., Henrich, P.P., Cowell, A.N., Gupta, P.,
1101 Stegman, M.L., Hoke, J.M., *et al.* (2017). A Variant PfCRT Isoform Can Contribute to *Plasmodium*
1102 *falciparum* Resistance to the First-Line Partner Drug Piperazine. *mBio* *8*.

1103 Divo, A.A., Geary, T.G., Davis, N.L., and Jensen, J.B. (1985). Nutritional requirements of *Plasmodium*
1104 *falciparum* in culture. I. Exogenously supplied dialyzable components necessary for continuous
1105 growth. *J Protozool* *32*, 59-64.

1106 Dondorp, A.M., Nosten, F., Yi, P., Das, D., Phyo, A.P., Tarning, J., Lwin, K.M., Ariey, F., Hanpithakpong,
1107 W., Lee, S.J., *et al.* (2009). Artemisinin resistance in *Plasmodium falciparum* malaria. *N Engl J Med* *361*,
1108 455-467.

1109 Duru, V., Khim, N., Leang, R., Kim, S., Domergue, A., Kloeung, N., Ke, S., Chy, S., Eam, R., Khean, C., *et*
1110 *al.* (2015). *Plasmodium falciparum* dihydroartemisinin-piperazine failures in Cambodia are
1111 associated with mutant K13 parasites presenting high survival rates in novel piperazine in vitro
1112 assays: retrospective and prospective investigations. *BMC Med* *13*, 305.

1113 Fennell, C., Babbitt, S., Russo, I., Wilkes, J., Ranford-Cartwright, L., Goldberg, D.E., and Doerig, C.
1114 (2009). PfelK1, a eukaryotic initiation factor 2alpha kinase of the human malaria parasite *Plasmodium*
1115 *falciparum*, regulates stress-response to amino-acid starvation. *Malar J* *8*, 99.

1116 Ferrari, V., and Cutler, D.J. (1990). Uptake of chloroquine by human erythrocytes. *Biochem Pharmacol*
1117 *39*, 753-762.

1118 Ferrari, V., and Cutler, D.J. (1991). Kinetics and thermodynamics of chloroquine and
1119 hydroxychloroquine transport across the human erythrocyte membrane. *Biochem Pharmacol* *41*, 23-
1120 30.

1121 Fitch, C.D., Ng, R.C., and Chevli, R. (1978). Erythrocyte surface: novel determinant of drug susceptibility
1122 in rodent malaria. *Antimicrob Agents Chemother* *14*, 185-193.

1123 Foley, M., and Tilley, L. (1998). Quinoline antimalarials: mechanisms of action and resistance and
1124 prospects for new agents. *Pharmacol Ther* 79, 55-87.

1125 Francis, S.E., Sullivan, D.J., Jr., and Goldberg, D.E. (1997). Hemoglobin metabolism in the malaria
1126 parasite *Plasmodium falciparum*. *Annu Rev Microbiol* 51, 97-123.

1127 Garten, M., Nasamu, A.S., Niles, J.C., Zimmerberg, J., Goldberg, D.E., and Beck, J.R. (2018). EXP2 is a
1128 nutrient-permeable channel in the vacuolar membrane of *Plasmodium* and is essential for protein
1129 export via PTEX. *Nat Microbiol* 3, 1090-1098.

1130 Ginsburg, H., Krugliak, M., Eidelman, O., and Cabantchik, Z.I. (1983). New permeability pathways
1131 induced in membranes of *Plasmodium falciparum* infected erythrocytes. *Mol Biochem Parasitol* 8,
1132 177-190.

1133 Gollmack, A., Henke, B., Bergmann, B., Wiechert, M., Erler, H., Blancke Soares, A., Spielmann, T., and
1134 Beitz, E. (2017). Substrate-analogous inhibitors exert antimalarial action by targeting the *Plasmodium*
1135 lactate transporter PffNT at nanomolar scale. *PLoS Pathog* 13, e1006172.

1136 Heiber, A., Kruse, F., Pick, C., Gruring, C., Flemming, S., Oberli, A., Schoeler, H., Retzlaff, S., Mesen-
1137 Ramirez, P., Hiss, J.A., *et al.* (2013). Identification of new PNEPs indicates a substantial non-PEXEL
1138 exportome and underpins common features in *Plasmodium falciparum* protein export. *PLoS Pathog* 9,
1139 e1003546.

1140 Hott, A., Casandra, D., Sparks, K.N., Morton, L.C., Castanares, G.G., Rutter, A., and Kyle, D.E. (2015).
1141 Artemisinin-resistant *Plasmodium falciparum* parasites exhibit altered patterns of development in
1142 infected erythrocytes. *Antimicrob Agents Chemother* 59, 3156-3167.

1143 Jida, M., Sanchez, C.P., Urgin, K., Ehrhardt, K., Mounien, S., Geyer, A., Elhabiri, M., Lanzer, M., and
1144 Davioud-Charvet, E. (2017). A Redox-Active Fluorescent pH Indicator for Detecting *Plasmodium*
1145 *falciparum* Strains with Reduced Responsiveness to Quinoline Antimalarial Drugs. *ACS Infect Dis* 3,
1146 119-131.

1147 Khoury, D.S., Cao, P., Zaloumis, S.G., Davenport, M.P., and Interdisciplinary Approaches to Malaria, C.
1148 (2020). Artemisinin Resistance and the Unique Selection Pressure of a Short-acting Antimalarial.
1149 *Trends Parasitol* 36, 884-887.

1150 Kirk, K., Horner, H.A., and Kirk, J. (1996). Glucose uptake in *Plasmodium falciparum*-infected
1151 erythrocytes is an equilibrative not an active process. *Mol Biochem Parasitol* 82, 195-205.

1152 Klonis, N., Creek, D.J., and Tilley, L. (2013). Iron and heme metabolism in *Plasmodium falciparum* and
1153 the mechanism of action of artemisinins. *Curr Opin Microbiol* 16, 722-727.

1154 Krishnan, A., and Soldati-Favre, D. (2021). Amino Acid Metabolism in Apicomplexan Parasites.
1155 *Metabolites* 11.

1156 Kucharski, M., Tripathi, J., Nayak, S., Zhu, L., Wirjanata, G., van der Pluijm, R.W., Dhorda, M., Dondorp,
1157 A., and Bozdech, Z. (2020). A comprehensive RNA handling and transcriptomics guide for high-
1158 throughput processing of *Plasmodium* blood-stage samples. *Malar J* 19, 363.

1159 Kumar, M., Skillman, K., and Duraisingh, M.T. (2020). Linking nutrient sensing and gene expression in
1160 *Plasmodium falciparum* blood-stage parasites. *Mol Microbiol*.

1161 Leang, R., Taylor, W.R., Bouth, D.M., Song, L., Tarning, J., Char, M.C., Kim, S., Witkowski, B., Duru, V.,
1162 Domergue, A., *et al.* (2015). Evidence of *Plasmodium falciparum* Malaria Multidrug Resistance to
1163 Artemisinin and Piperaquine in Western Cambodia: Dihydroartemisinin-Piperaquine Open-Label
1164 Multicenter Clinical Assessment. *Antimicrob Agents Chemother* 59, 4719-4726.

1165 Lemieux, J.E., Gomez-Escobar, N., Feller, A., Carret, C., Amambua-Ngwa, A., Pinches, R., Day, F., Kyes,
1166 S.A., Conway, D.J., Holmes, C.C., *et al.* (2009). Statistical estimation of cell-cycle progression and
1167 lineage commitment in *Plasmodium falciparum* reveals a homogeneous pattern of transcription in ex
1168 vivo culture. *Proc Natl Acad Sci U S A* 106, 7559-7564.

1169 Lingelbach, K., and Joiner, K.A. (1998). The parasitophorous vacuole membrane surrounding
1170 *Plasmodium* and *Toxoplasma*: an unusual compartment in infected cells. *J Cell Sci* 111 (Pt 11), 1467-
1171 1475.

1172 Lisewski, A.M., Quiros, J.P., Ng, C.L., Adikesavan, A.K., Miura, K., Putluri, N., Eastman, R.T., Scandfield,
1173 D., Regenbogen, S.J., Altenhofen, L., *et al.* (2014). Supergenomic network compression and the
1174 discovery of EXP1 as a glutathione transferase inhibited by artesunate. *Cell* *158*, 916-928.

1175 Liu, J., Istvan, E.S., Gluzman, I.Y., Gross, J., and Goldberg, D.E. (2006). Plasmodium falciparum ensures
1176 its amino acid supply with multiple acquisition pathways and redundant proteolytic enzyme systems.
1177 *Proc Natl Acad Sci U S A* *103*, 8840-8845.

1178 Low, L.M., Azasi, Y., Sherling, E.S., Garten, M., Zimmerberg, J., Tsuboi, T., Brzostowski, J., Mu, J.,
1179 Blackman, M.J., and Miller, L.H. (2019). Deletion of Plasmodium falciparum Protein RON3 Affects the
1180 Functional Translocation of Exported Proteins and Glucose Uptake. *mBio* *10*.

1181 Macomber, P.B., O'Brien, R.L., and Hahn, F.E. (1966). Chloroquine: physiological basis of drug
1182 resistance in Plasmodium berghei. *Science* *152*, 1374-1375.

1183 MacRae, J.I., Dixon, M.W., Dearnley, M.K., Chua, H.H., Chambers, J.M., Kenny, S., Bottova, I., Tilley, L.,
1184 and McConville, M.J. (2013). Mitochondrial metabolism of sexual and asexual blood stages of the
1185 malaria parasite Plasmodium falciparum. *BMC Biol* *11*, 67.

1186 Mesen-Ramirez, P., Bergmann, B., Tran, T.T., Garten, M., Stacker, J., Naranjo-Prado, I., Hohn, K.,
1187 Zimmerberg, J., and Spielmann, T. (2019). EXP1 is critical for nutrient uptake across the
1188 parasitophorous vacuole membrane of malaria parasites. *PLoS Biol* *17*, e3000473.

1189 Mesen-Ramirez, P., Reinsch, F., Blancke Soares, A., Bergmann, B., Ullrich, A.K., Tenzer, S., and
1190 Spielmann, T. (2016). Stable Translocation Intermediates Jam Global Protein Export in Plasmodium
1191 falciparum Parasites and Link the PTEX Component EXP2 with Translocation Activity. *PLoS Pathog* *12*,
1192 e1005618.

1193 Mi-Ichi, F., Kano, S., and Mitamura, T. (2007). Oleic acid is indispensable for intraerythrocytic
1194 proliferation of Plasmodium falciparum. *Parasitology* *134*, 1671-1677.

1195 Mitamura, T., Hanada, K., Ko-Mitamura, E.P., Nishijima, M., and Horii, T. (2000). Serum factors
1196 governing intraerythrocytic development and cell cycle progression of Plasmodium falciparum.
1197 *Parasitol Int* *49*, 219-229.

1198 Mok, S., Ashley, E.A., Ferreira, P.E., Zhu, L., Lin, Z., Yeo, T., Chotivanich, K., Imwong, M.,
1199 Pukrittayakamee, S., Dhorda, M., *et al.* (2015). Drug resistance. Population transcriptomics of human
1200 malaria parasites reveals the mechanism of artemisinin resistance. *Science* *347*, 431-435.

1201 Mok, S., Imwong, M., Mackinnon, M.J., Sim, J., Ramadoss, R., Yi, P., Mayxay, M., Chotivanich, K., Liong,
1202 K.Y., Russell, B., *et al.* (2011). Artemisinin resistance in Plasmodium falciparum is associated with an
1203 altered temporal pattern of transcription. *BMC Genomics* *12*, 391.

1204 Mok, S., Stokes, B.H., Gnadig, N.F., Ross, L.S., Yeo, T., Amaratunga, C., Allman, E., Solyakov, L., Bottrill,
1205 A.R., Tripathi, J., *et al.* (2021). Artemisinin-resistant K13 mutations rewire Plasmodium falciparum's
1206 intra-erythrocytic metabolic program to enhance survival. *Nat Commun* *12*, 530.

1207 Nair, S., Li, X., Arya, G.A., McDew-White, M., Ferrari, M., Nosten, F., and Anderson, T.J.C. (2018).
1208 Fitness Costs and the Rapid Spread of kelch13-C580Y Substitutions Conferring Artemisinin Resistance.
1209 *Antimicrob Agents Chemother* *62*.

1210 Nessel, T., Beck, J.M., Rayatpisheh, S., Jami-Alahmadi, Y., Wohlschlegel, J.A., Goldberg, D.E., and Beck,
1211 J.R. (2020). EXP1 is required for organisation of EXP2 in the intraerythrocytic malaria parasite vacuole.
1212 *Cell Microbiol* *22*, e13168.

1213 Pillai, A.D., Nguiragool, W., Lyko, B., Dolinta, K., Butler, M.M., Nguyen, S.T., Peet, N.P., Bowlin, T.L.,
1214 and Desai, S.A. (2012). Solute restriction reveals an essential role for clag3-associated channels in
1215 malaria parasite nutrient acquisition. *Mol Pharmacol* *82*, 1104-1114.

1216 Rocamora, F., Zhu, L., Liong, K.Y., Dondorp, A., Miotto, O., Mok, S., and Bozdech, Z. (2018). Oxidative
1217 stress and protein damage responses mediate artemisinin resistance in malaria parasites. *PLoS Pathog*
1218 *14*, e1006930.

1219 Sachanonta, N., Chotivanich, K., Chaisri, U., Turner, G.D., Ferguson, D.J., Day, N.P., and Pongponratn,
1220 E. (2011). Ultrastructural and real-time microscopic changes in P. falciparum-infected red blood cells
1221 following treatment with antimalarial drugs. *Ultrastruct Pathol* *35*, 214-225.

1222 Saliba, K.J., Allen, R.J., Zissis, S., Bray, P.G., Ward, S.A., and Kirk, K. (2003). Acidification of the malaria
1223 parasite's digestive vacuole by a H⁺-ATPase and a H⁺-pyrophosphatase. *J Biol Chem* 278, 5605-5612.

1224 Saunders, D.L., Vanachayangkul, P., Lon, C., Program, U.S.A.M.M.R., National Center for Parasitology,
1225 E., Malaria, C., and Royal Cambodian Armed, F. (2014). Dihydroartemisinin-piperazine failure in
1226 Cambodia. *N Engl J Med* 371, 484-485.

1227 Schallig, H.D., Tinto, H., Sawa, P., Kaur, H., Duparc, S., Ishengoma, D.S., Magnussen, P., Alifrangis, M.,
1228 and Sutherland, C.J. (2017). Randomised controlled trial of two sequential artemisinin-based
1229 combination therapy regimens to treat uncomplicated falciparum malaria in African children: a
1230 protocol to investigate safety, efficacy and adherence. *BMJ Glob Health* 2, e000371.

1231 Schneider, C.A., Rasband, W.S., and Eliceiri, K.W. (2012). NIH Image to ImageJ: 25 years of image
1232 analysis. *Nat Methods* 9, 671-675.

1233 Schwenk, R.W., Holloway, G.P., Luiken, J.J., Bonen, A., and Glatz, J.F. (2010). Fatty acid transport across
1234 the cell membrane: regulation by fatty acid transporters. *Prostaglandins Leukot Essent Fatty Acids* 82,
1235 149-154.

1236 Semba, R.D., Shardell, M., Sakr Ashour, F.A., Moaddel, R., Trehan, I., Maleta, K.M., Ordiz, M.I.,
1237 Kraemer, K., Khadeer, M.A., Ferrucci, L., *et al.* (2016). Child Stunting is Associated with Low Circulating
1238 Essential Amino Acids. *EBioMedicine* 6, 246-252.

1239 Siddiqui, G., Srivastava, A., Russell, A.S., and Creek, D.J. (2017). Multi-omics Based Identification of
1240 Specific Biochemical Changes Associated With Pfk13-Mutant Artemisinin-Resistant Plasmodium
1241 falciparum. *J Infect Dis* 215, 1435-1444.

1242 Spielmann, T., Ferguson, D.J., and Beck, H.P. (2003). *etramps*, a new Plasmodium falciparum gene
1243 family coding for developmentally regulated and highly charged membrane proteins located at the
1244 parasite-host cell interface. *Mol Biol Cell* 14, 1529-1544.

1245 Spielmann, T., Gras, S., Sabitzki, R., and Meissner, M. (2020). Endocytosis in Plasmodium and
1246 Toxoplasma Parasites. *Trends Parasitol* 36, 520-532.

1247 Spielmann, T., Montagna, G.N., Hecht, L., and Matuschewski, K. (2012). Molecular make-up of the
1248 Plasmodium parasitophorous vacuolar membrane. *Int J Med Microbiol* 302, 179-186.

1249 Straimer, J., Gnadig, N.F., Stokes, B.H., Ehrenberger, M., Crane, A.A., and Fidock, D.A. (2017).
1250 Plasmodium falciparum K13 Mutations Differentially Impact Ozonide Susceptibility and Parasite
1251 Fitness In Vitro. *mBio* 8.

1252 Straimer, J., Gnadig, N.F., Witkowski, B., Amaratunga, C., Duru, V., Ramadani, A.P., Dacheux, M., Khim,
1253 N., Zhang, L., Lam, S., *et al.* (2015). Drug resistance. K13-propeller mutations confer artemisinin
1254 resistance in Plasmodium falciparum clinical isolates. *Science* 347, 428-431.

1255 Struck, N.S., de Souza Dias, S., Langer, C., Marti, M., Pearce, J.A., Cowman, A.F., and Gilberger, T.W.
1256 (2005). Re-defining the Golgi complex in Plasmodium falciparum using the novel Golgi marker
1257 PfGRASP. *J Cell Sci* 118, 5603-5613.

1258 Sutherland, C.J., Henrici, R.C., and Artavanis-Tsakonas, K. (2020). Artemisinin susceptibility in the
1259 malaria parasite Plasmodium falciparum: propellers, adaptor proteins and the need for cellular
1260 healing. *FEMS Microbiol Rev*.

1261 Tanabe, K. (1990). Glucose transport in malaria infected erythrocytes. *Parasitol Today* 6, 225-229.

1262 Taylor, H.M., McRobert, L., Grainger, M., Sicard, A., Dluzewski, A.R., Hopp, C.S., Holder, A.A., and
1263 Baker, D.A. (2010). The malaria parasite cyclic GMP-dependent protein kinase plays a central role in
1264 blood-stage schizogony. *Eukaryot Cell* 9, 37-45.

1265 Tonkin, C.J., van Dooren, G.G., Spurck, T.P., Struck, N.S., Good, R.T., Handman, E., Cowman, A.F., and
1266 McFadden, G.I. (2004). Localization of organellar proteins in Plasmodium falciparum using a novel set
1267 of transfection vectors and a new immunofluorescence fixation method. *Mol Biochem Parasitol* 137,
1268 13-21.

1269 Uwimana, A., Legrand, E., Stokes, B.H., Ndikumana, J.M., Warsame, M., Umulisa, N., Ngamije, D.,
1270 Munyaneza, T., Mazarati, J.B., Munguti, K., *et al.* (2020). Emergence and clonal expansion of in vitro
1271 artemisinin-resistant Plasmodium falciparum kelch13 R561H mutant parasites in Rwanda. *Nat Med*.

1272 van der Pluijm, R.W., Imwong, M., Chau, N.H., Hoa, N.T., Thuy-Nhien, N.T., Thanh, N.V., Jittamala, P.,
1273 Hanboonkunupakarn, B., Chutasmit, K., Saelow, C., *et al.* (2019). Determinants of dihydroartemisinin-
1274 piperaquine treatment failure in *Plasmodium falciparum* malaria in Cambodia, Thailand, and Vietnam:
1275 a prospective clinical, pharmacological, and genetic study. *Lancet Infect Dis* 19, 952-961.

1276 van der Pluijm, R.W., Tripura, R., Hoglund, R.M., Pyae Phyo, A., Lek, D., Ul Islam, A., Anvikar, A.R.,
1277 Satpathi, P., Satpathi, S., Behera, P.K., *et al.* (2020). Triple artemisinin-based combination therapies
1278 versus artemisinin-based combination therapies for uncomplicated *Plasmodium falciparum* malaria:
1279 a multicentre, open-label, randomised clinical trial. *Lancet*.

1280 Whittam, R. (1960). The high permeability of human red cells to adenine and hypoxanthine and their
1281 ribosides. *J Physiol* 154, 614-623.

1282 WHO, W.H.O. (2019). World Malaria Report ([https://www.who.int/](https://www.who.int/publications-detail/world-malaria-report-2019)
1283 [publications-detail/world-](https://www.who.int/publications-detail/world-malaria-report-2019)
1284 [malaria-report-2019](https://www.who.int/publications-detail/world-malaria-report-2019) (2019)
1285 World Health Organization).

1285 Witkowski, B., Khim, N., Chim, P., Kim, S., Ke, S., Kloeung, N., Chy, S., Duong, S., Leang, R., Ringwald,
1286 P., *et al.* (2013). Reduced artemisinin susceptibility of *Plasmodium falciparum* ring stages in western
1287 Cambodia. *Antimicrob Agents Chemother* 57, 914-923.

1288 Wong, W., Bai, X.C., Sleebs, B.E., Triglia, T., Brown, A., Thompson, J.K., Jackson, K.E., Hanssen, E.,
1289 Marapana, D.S., Fernandez, I.S., *et al.* (2017). Mefloquine targets the *Plasmodium falciparum* 80S
1290 ribosome to inhibit protein synthesis. *Nat Microbiol* 2, 17031.

1291 Woodrow, C.J., Burchmore, R.J., and Krishna, S. (2000). Hexose permeation pathways in *Plasmodium*
1292 *falciparum*-infected erythrocytes. *Proc Natl Acad Sci U S A* 97, 9931-9936.

1293 Woodrow, C.J., and White, N.J. (2017). The clinical impact of artemisinin resistance in Southeast Asia
1294 and the potential for future spread. *FEMS Microbiol Rev* 41, 34-48.

1295 Yamada, K., Saito, M., Matsuoka, H., and Inagaki, N. (2007). A real-time method of imaging glucose
1296 uptake in single, living mammalian cells. *Nat Protoc* 2, 753-762.

1297 Yang, T., Yeoh, L.M., Tutor, M.V., Dixon, M.W., McMillan, P.J., Xie, S.C., Bridgford, J.L., Gillett, D.L.,
1298 Duffy, M.F., Ralph, S.A., *et al.* (2019). Decreased K13 Abundance Reduces Hemoglobin Catabolism and
1299 Proteotoxic Stress, Underpinning Artemisinin Resistance. *Cell Rep* 29, 2917-2928 e2915.

1300 Yayon, A., Cabantchik, Z.I., and Ginsburg, H. (1984). Identification of the acidic compartment of
1301 *Plasmodium falciparum*-infected human erythrocytes as the target of the antimalarial drug
1302 chloroquine. *EMBO J* 3, 2695-2700.

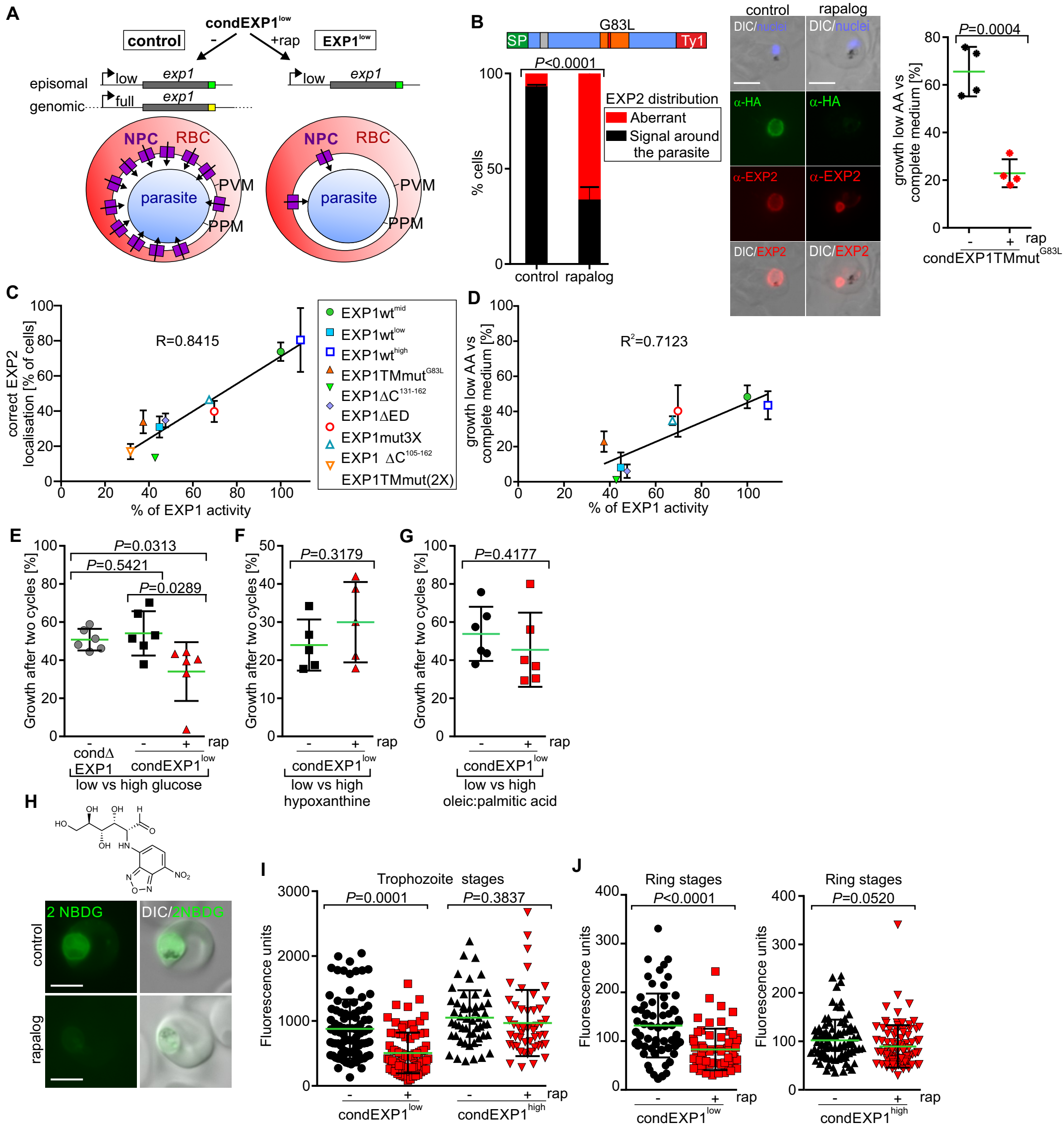
1303 Yoo, H.C., Yu, Y.C., Sung, Y., and Han, J.M. (2020). Glutamine reliance in cell metabolism. *Exp Mol Med*
1304 52, 1496-1516.

1305 Zhang, M., Gallego-Delgado, J., Fernandez-Arias, C., Waters, N.C., Rodriguez, A., Tsuji, M., Wek, R.C.,
1306 Nussenzweig, V., and Sullivan, W.J., Jr. (2017). Inhibiting the *Plasmodium* eIF2alpha Kinase PK4
1307 Prevents Artemisinin-Induced Latency. *Cell Host Microbe* 22, 766-776 e764.

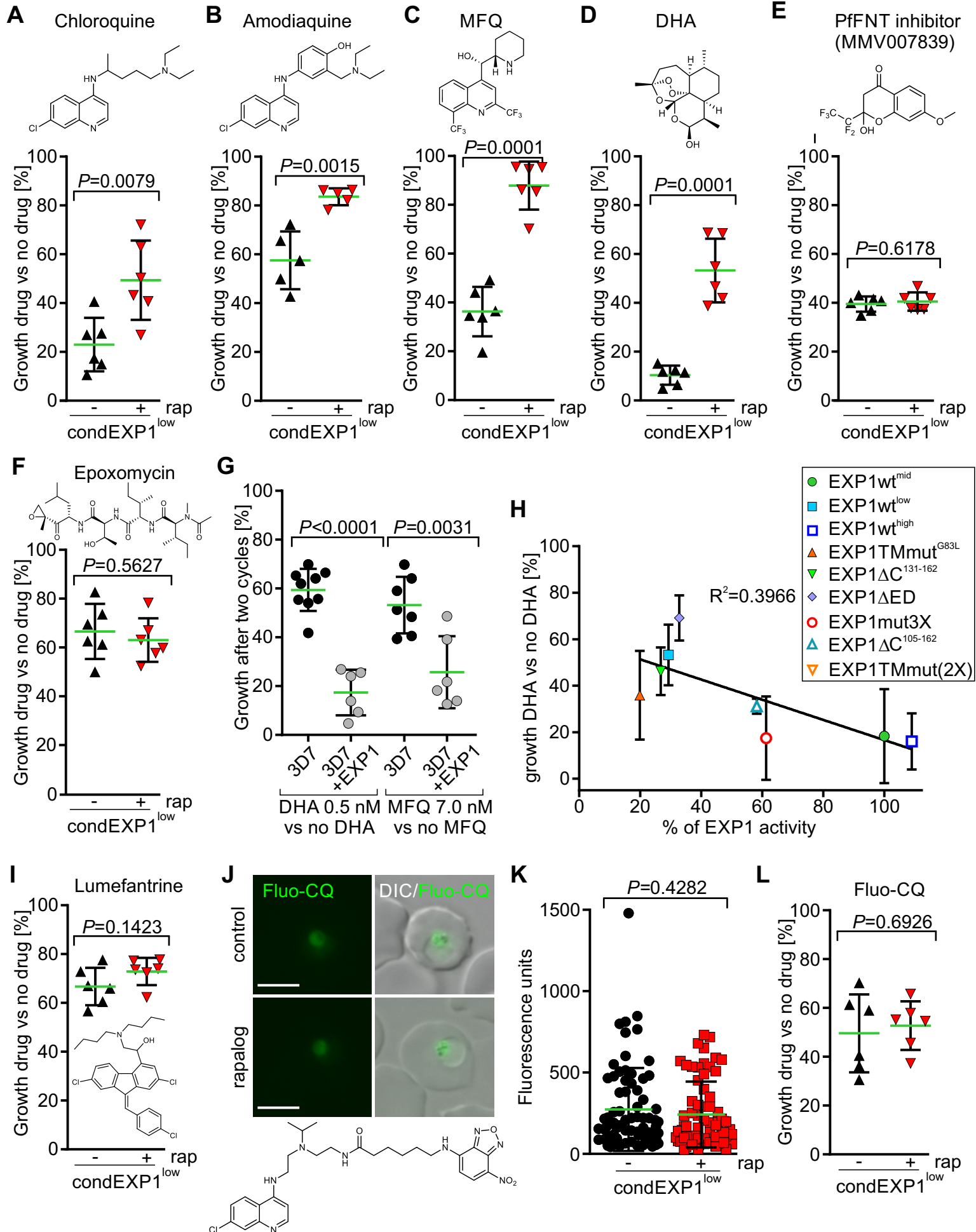
1308 Zhu, L., Tripathi, J., Rocamora, F.M., Miotto, O., van der Pluijm, R., Voss, T.S., Mok, S., Kwiatkowski,
1309 D.P., Nosten, F., Day, N.P.J., *et al.* (2018). The origins of malaria artemisinin resistance defined by a
1310 genetic and transcriptomic background. *Nat Commun* 9, 5158.

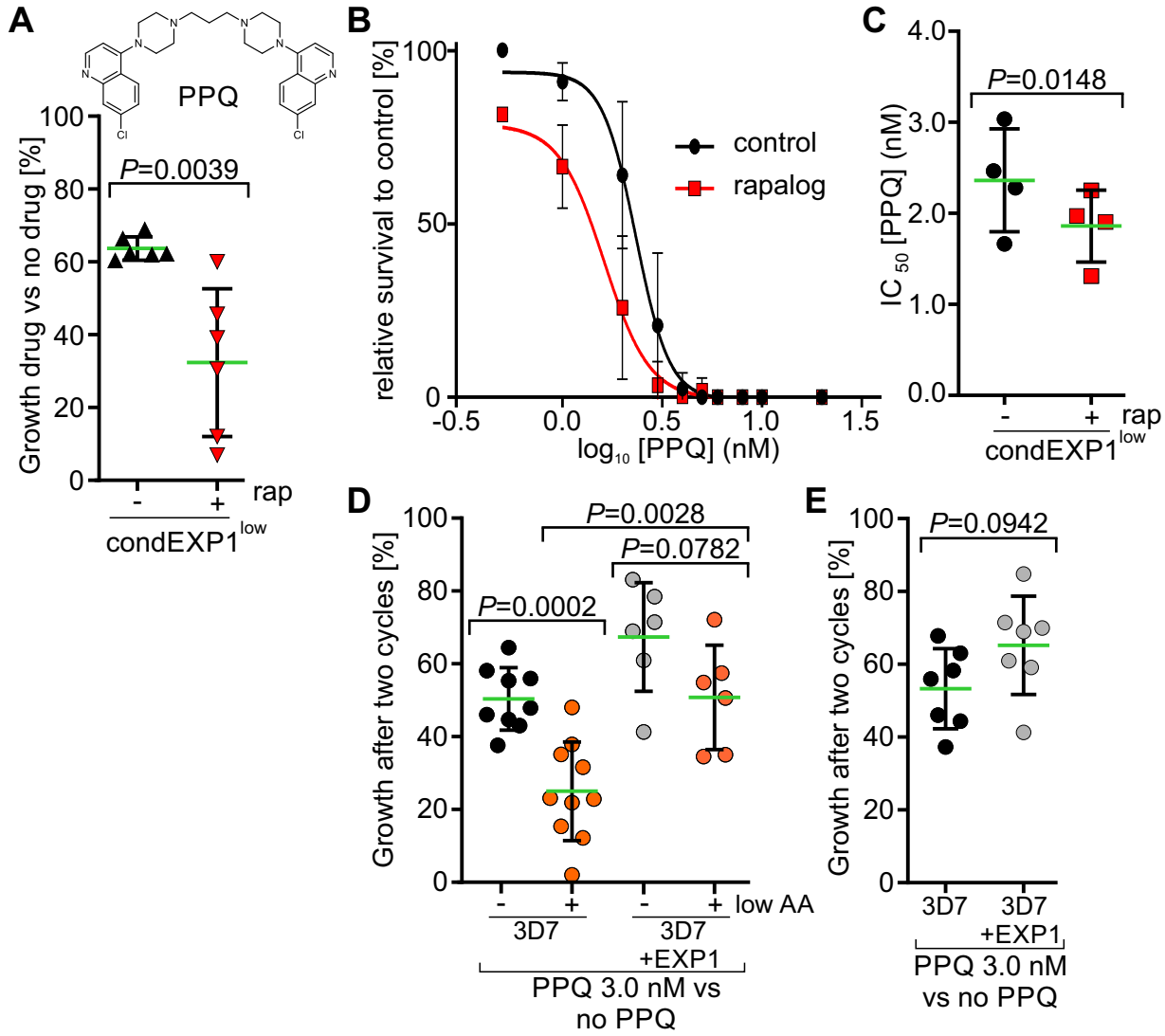
1311 Zhu, L., van der Pluijm, R.W., Kucharski, M., Nayak, S., Tripathi, J., Nosten, F., Faiz, A., Amaratunga, C.,
1312 Lek, D., Ashley, E.A., *et al.* (2021). The mechanism of artemisinin resistance of *Plasmodium*
1313 *falciparum* malaria parasites originates in their initial transcriptional response. *bioRxiv*,
1314 2021.2005.2017.444396.

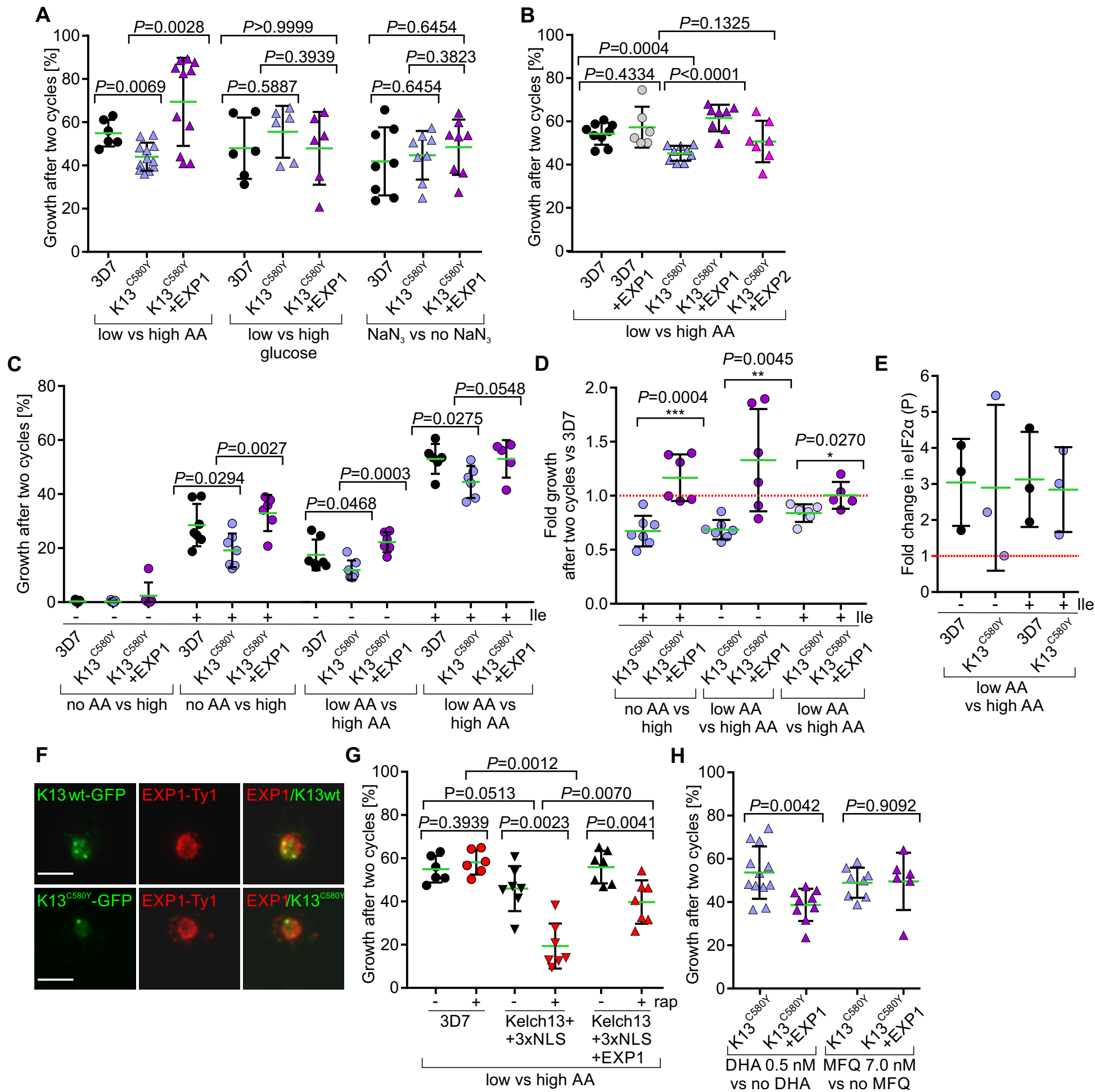
1315

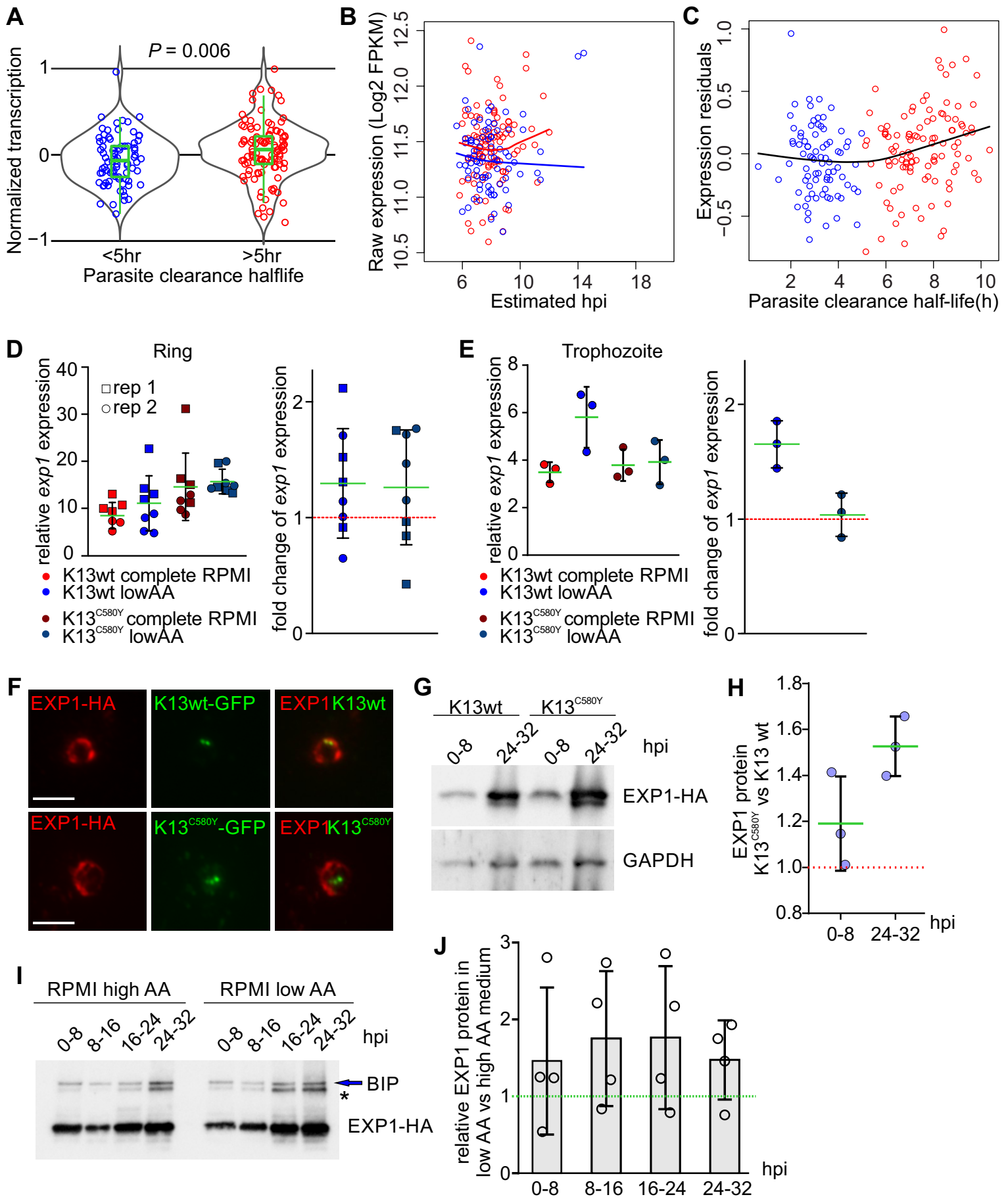


Mesen-Ramirez et al Fig. 2

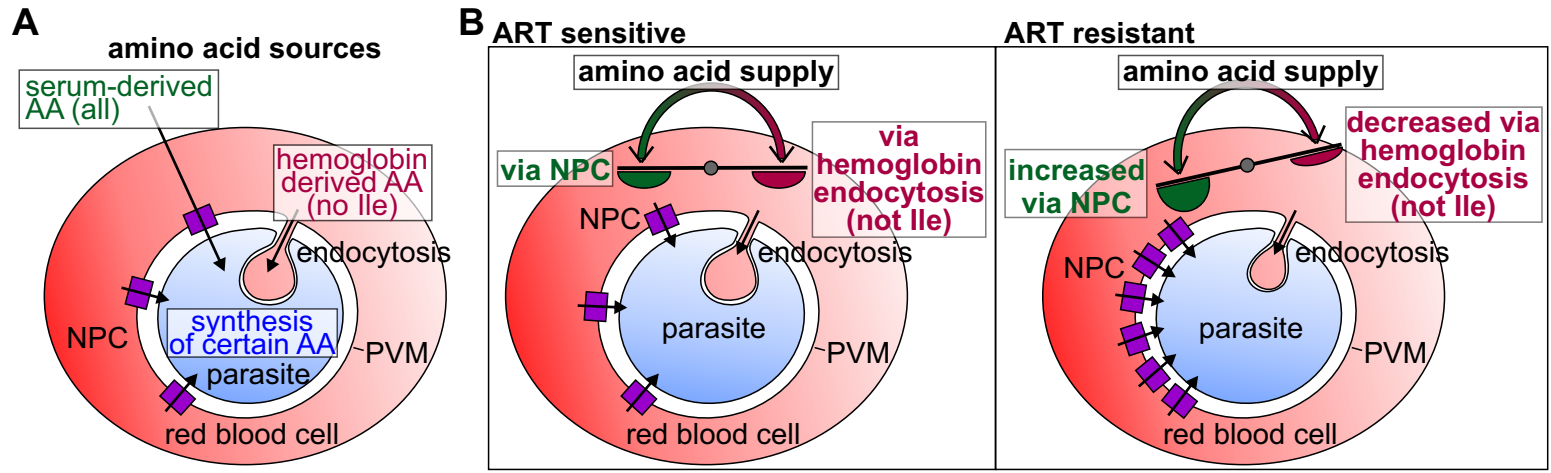








Mesen-Ramirez et al Fig. 6



Supplemental information

**The parasitophorous vacuole nutrient channel is p
critical for drug access in malaria parasites and
modulates the artemisinin resistance fitness cost**

Paolo Mesén-Ramírez, Bärbel Bergmann, Mourad Elhabiri, Lei Zhu, Heidrun von Thien, Carolina Castro-Peña, Tim-Wolf Gilberger, Elisabeth Davioud-Charvet, Zbynec Bozdech, Anna Bachmann, and Tobias Spielmann

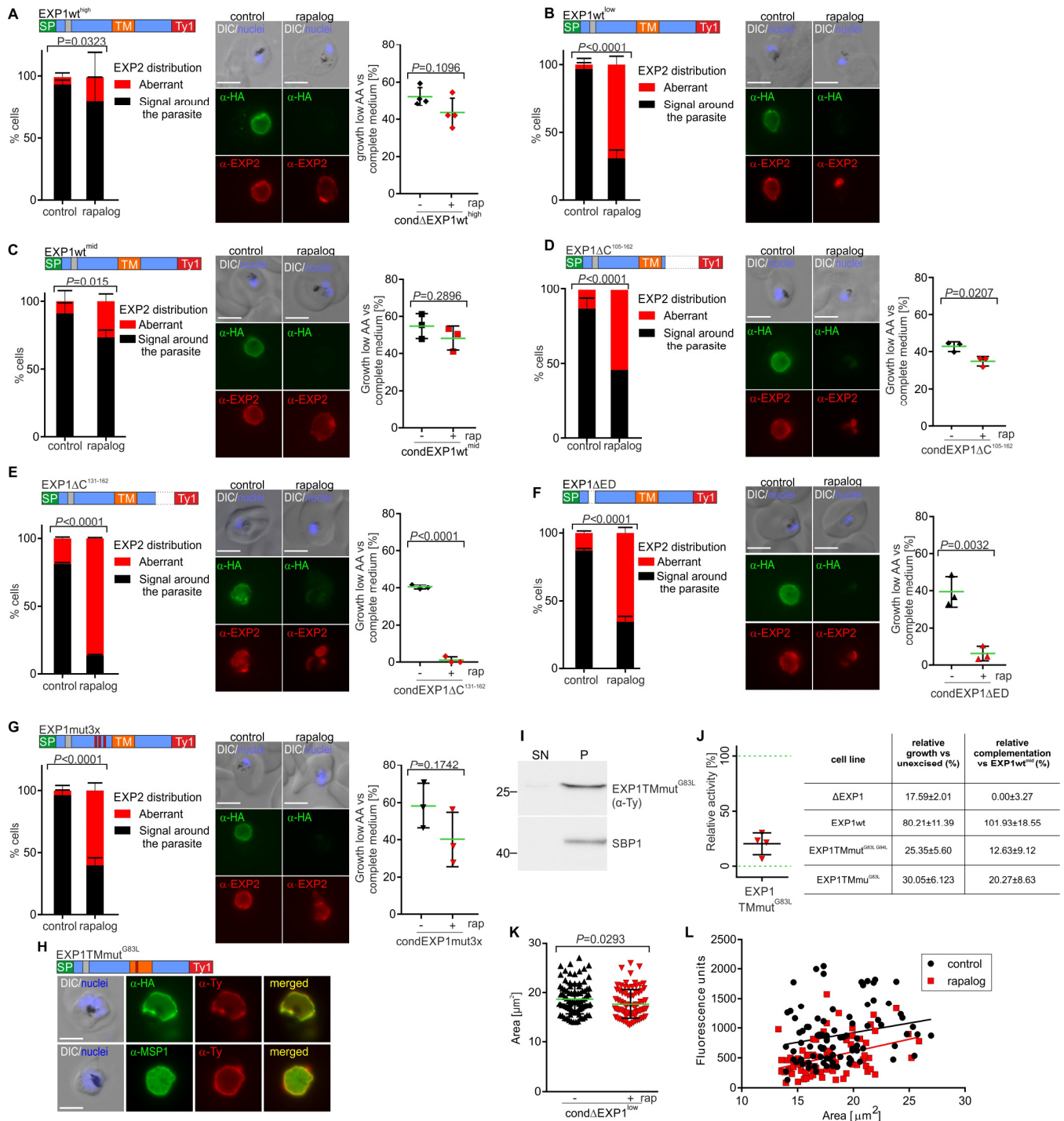


Figure S1. Correlation of EXP1 activity with nutrient permeability and EXP2 phenotypes. Related to Figure 1.

(A-G) Left to right, distribution of EXP2 at the PVM (phenotype quantification and representative IFA images) of age-matched trophozoites relying on the schematically shown modified EXP1 (rapalog) compared to the controls still expressing endogenous EXP1. Right, relative growth after 96 h under low amino acids compared to standard medium of parasites relying on the indicated modified EXP1. α-HA: floxed endogenous EXP1-HA; α-EXP2 endogenous EXP2. DIC, differential interference contrast; scale bars, 5 μm; DAPI, nuclei. EXP2 distribution: mean of n=52 control and n=67 rapalog-treated parasites

(A), n=67 and n=99 (B), n=64 and n=80 (C) n=54 and n=59 (D), n=55 and n=56 (E), n=105 and n=159 (F), n=63 and n=79 (G) from a total of 2 independent experiments; *P* values calculated with Fischer's exact test. Relative growth experiments: mean, green line of $n \geq 3$ independent experiments; *P* values calculated with a two-tailed unpaired *t* test. Error bars indicate SD. For (B) relative growth under low amino acid was previously determined (Mesen-Ramirez et al., 2019). (H) IFA images of cond Δ EXP1 schizont stages expressing EXP1TMmut^{G83L}-Ty (schematic above panel) probed with α -HA and α -Ty1. Endogenous (EXP1-HA) and the episomal EXP1TMmut^{G83L} both localise to the PVM. α -MSP1 (MSP1) labels the PPM. DAPI, nuclei; scale bars, 5 μ m. (I) Immunoblot of extracts of cell line in (G) showing saponin pellet (P, containing parasite internal and membrane proteins) and supernatant (SN, containing soluble PV and host cell content). α -Ty detects EXP1TMmut^{G83L}-Ty; α -SBP1 control membrane protein. (J) Relative activity of the construct EXP1TMmut^{G83L}-Ty. Each data point (red triangle) indicates growth of rapalog-treated versus growth of control parasites at day 5 of growth assay relative to the growth of parasites expressing an EXP1wt-Ty construct²³ which was set as 100% (upper dotted green line). Growth of Δ EXP1 was set to 0% (lower dotted green line); n=4 independent experiments. Error bars indicate SD. Values for every cell line are summarised in table. (K) Area (μ m²) of control and EXP1^{low} (rapalog) age-matched trophozoites analysed in Figure 1I. Mean (green line) of n=91 (control) and n=80 (rapalog) parasites from 3 independent experiments is shown. (L) Correlation of the 2-NBDG fluorescence intensity versus area of control and EXP1^{low} (rapalog) age-matched trophozoites analyzed in (K) and Figure 1I. *P* values indicated (two-tailed unpaired *t* test).

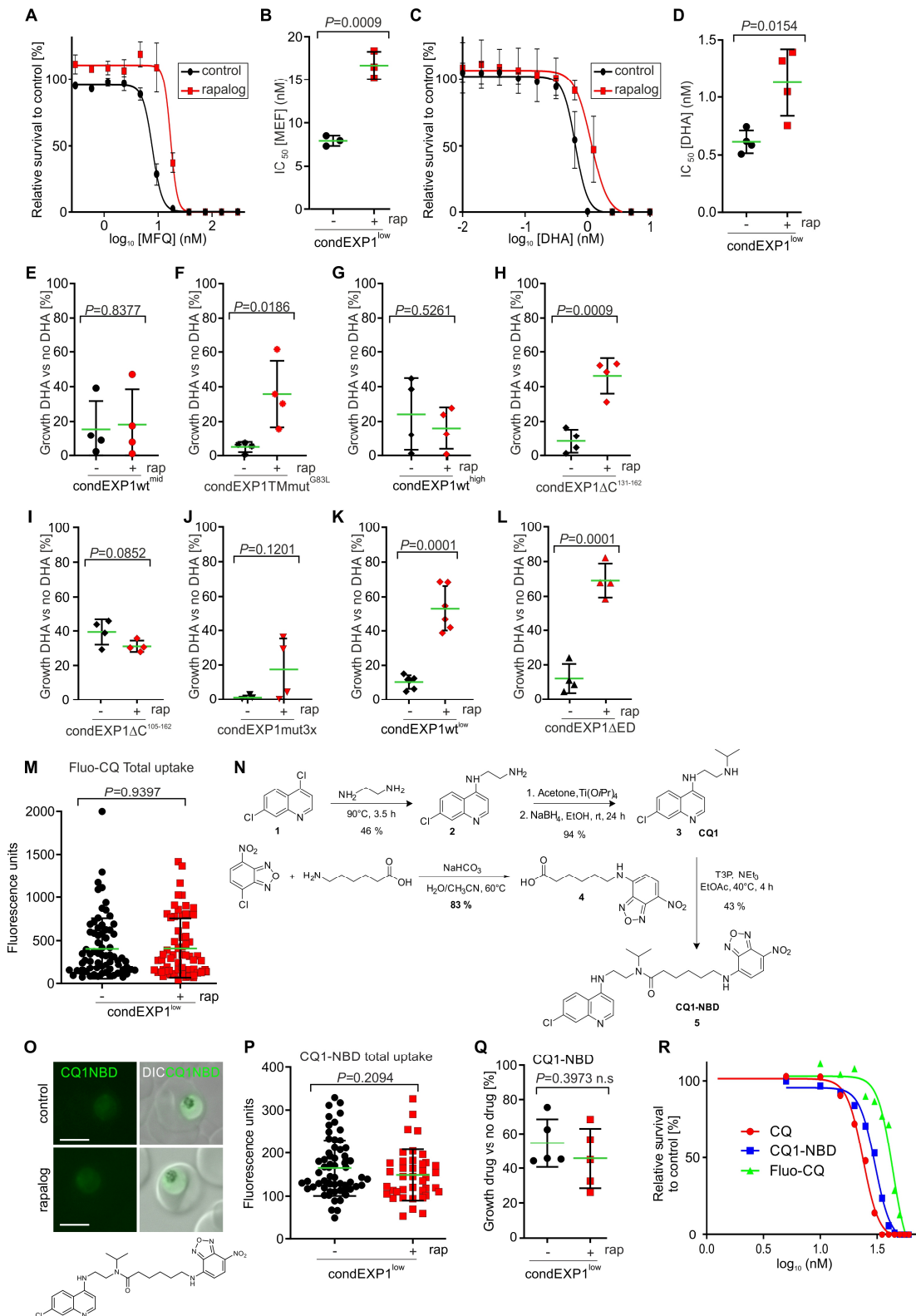


Figure S2. Activity of NPCs influences sensitivity to antimalarial drugs. Related to Figure 2.

(A-D) Curves of dose-dependent survival after 96 h of control condEXP1^{low} and EXP1^{low} (rapalog) parasites treated with increasing concentrations (log) of MFQ (0-300 nM) (A) and DHA (0-10 nM) (C). Mean of $n=3$ independent experiments. MFQ and DHA IC_{50}^{96} values (B, D) calculated from (A) and (C)

respectively. Mean (green line) of $n=3$ experiments. (E-L) Relative growth after 96 h of control (-rap) and parasites relying on the indicated EXP1 modified construct (+rap) when exposed to a IC_{50}^{96} of DHA compared to growth in medium without the drug. Mean, green line of $n \geq 3$ independent experiments; P values calculated with a two-tailed unpaired t test. (M) Quantification of Fluo-CQ total fluorescence (cytosolic and food vacuole uptake) in control (-rap) and EXP1^{low} (+rap) age-matched trophozoites shown in Figure 2K. Mean (green line) of $n=73$ (-rap) and $n=67$ (+rap) derived from three independent experiments. (N) Synthetic route to prepare CQ1-NBD. Nucleophilic aromatic substitution of the 4-chlorine of 4,7-dichloroquinoline (1) by ethylenediamine first led to *N*-(7-chloroquinolin-4-yl)ethyl-1,2-diamine (2). Compound 2 was then reacted in a one-step reductive amination with acetone to afford compound 3 (CQ1) in the presence of titanium isopropylate (IV) and sodium borohydride as reductive reagent. The final step for CQ1-NBD is a coupling reaction between CQ1 and an NBD-linker 4 (i.e. NBD-6-aminohexanoic acid precursor 4 which was prepared in 77% yield by a nucleophilic substitution reaction between 6-aminohexanoic acid and NBD-chloride in the presence of excess of sodium bicarbonate) accomplished with 3 equivalents of T3P (propanephosphonic acid anhydride) in the presence of 3 equivalents of NEt_3 at 40°C. (O) Live cell images of EXP1^{low} (rapalog) or control parasites after CQ1-NBD uptake. The structural formula of CQ1-NBD is depicted. DIC, differential interference contrast; scale bars, 5 μm . (P) Quantification of CQ1-NBD total fluorescence (cytosolic uptake) in control (-rap) and EXP1^{low} (+rap) age-matched trophozoites. Mean (green line) of $n=63$ (-rap) and $n=40$ (+rap) from 3 independent experiments. (Q) Relative growth after two cycles (96h) of EXP1^{low} (+rap) compared to controls (-rap) parasites exposed to IC_{50}^{96h} of CQ1-NBD versus growth without the drug. Mean (green line) of 5 biological replicates derived from at least two occasions is shown. P values indicated (two-tailed unpaired t test). (R) Curves of dose-dependent survival of 3D7 parasites treated with increasing concentrations (log) of CQ, Fluo-CQ and CQ1-NBD for 48 hours.

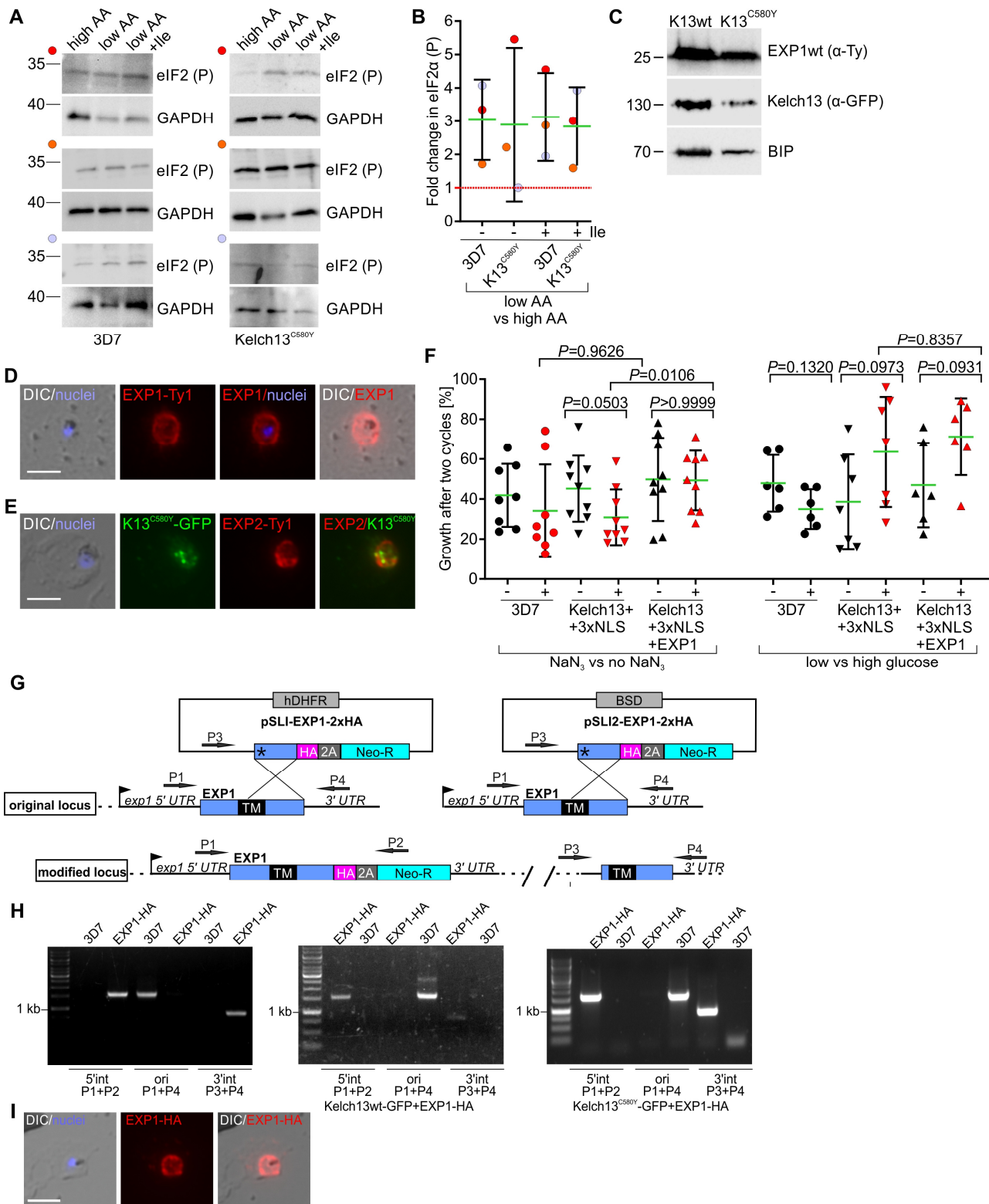


Figure S3. EXP1 levels compensate amino acid deficit in ART^R parasites. Related to Figures 4 and 5.

(A) Immunoblots of protein extracts from saponin pellets from 3D7 and Kelch13^{C580Y} ring stages cultured in medium with high AA concentration (RPMI standard), low AA (1:50 amino acid concentration of RPMI) ± isoleucine (Ile) (382 μM) probed with α-eIF2α (P) (phosphorylated eIF2α) and α-GAPDH (loading control). (B) Fold change of eIF2α (P) under low AA ± Ile relative to high AA (red line) quantified by

densitometry from blots shown in (A). eIF2 α (P) was normalised to GAPDH. n=3 independent experiments (colors denote experiments in (A)). (C) Immunoblot of lysates of parasites shown in Figure 4F probed with α -GFP (Kelch13wt and Kelch13C580Y-GFP), α -Ty (EXP1-Ty^{high}) and α -BIP (loading control). The marker is indicated in kDa. (D, E) Representative immunofluorescence images of 3D7 wild type parasites expressing EXP1-Ty^{high} (D) and Kelch13^{C580Y}-GFP parasites expressing EXP2-Ty^{high} (E). Acetone -fixed parasites were probed with α -GFP to detect endogenous Kelch13 and α -Ty for episomal EXP1-Ty and EXP2-Ty. DAPI, nuclei; DIC, differential interference contrast; scale bars, 5 μ m. (F) Relative growth after 2 cycles of the indicated parasite lines grown in medium containing sodium azide (NaN₃) versus growth in medium without NaN₃ (left) and in glucose-limited medium versus growth in complete medium (right). Cell lines were incubated \pm rapalog in the corresponding media and analysed in parallel to experiments in Figure 4G. Mean (green line) of n \geq 6 biological replicates obtained in at least n=3 independent experiments. Error bars indicate SD and *P* values were calculated with a non-parametric (Mann-Whitney) two-tailed t-test. (G) Left, schematic of representation of SLI strategy (Birnbaum et al., 2017) to generate parasites expressing endogenous HA-tagged EXP1. Plasmid pSLI-EXP1-2xHA and pSLI2-EXP1-HA, original and modified locus after integration are shown. Arrows, primers P1, P2, P3 and P4. (H) PCR on gDNA of EXP1-HA and 3D7 parasites (left), Kelch13wt +EXP1-HA (middle) and Kelch13^{C580Y}+EXP1-HA (right) using the primers indicated confirming: 5'Int, 5' integration; ori, absence of 'original locus'; 3'Int, 3' integration. HA, double hemagglutinin; hDHFR: human dihydrofolate reductase; Neo: neomycin phosphotransferase; BSD: blasticidine deaminase; asterisk, in frame stop codon; T2A, skip peptide; TM, transmembrane domain. (I) Representative immunofluorescence images of parasites expressing endogenous HA-tagged EXP1. Acetone -fixed parasites were probed with α -HA to detect endogenous EXP1. DAPI, nuclei; DIC, differential interference contrast; scale bars, 5 μ m.

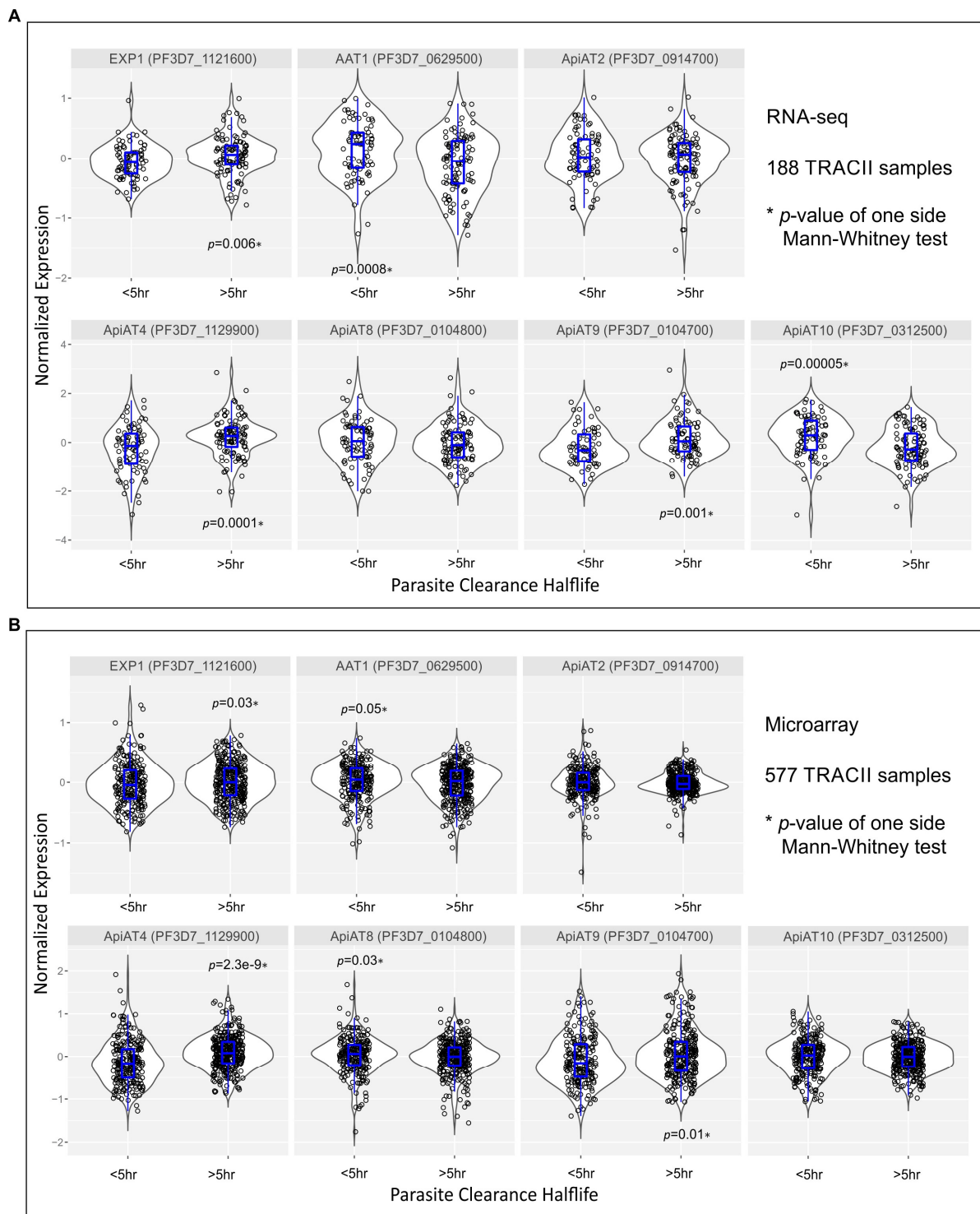
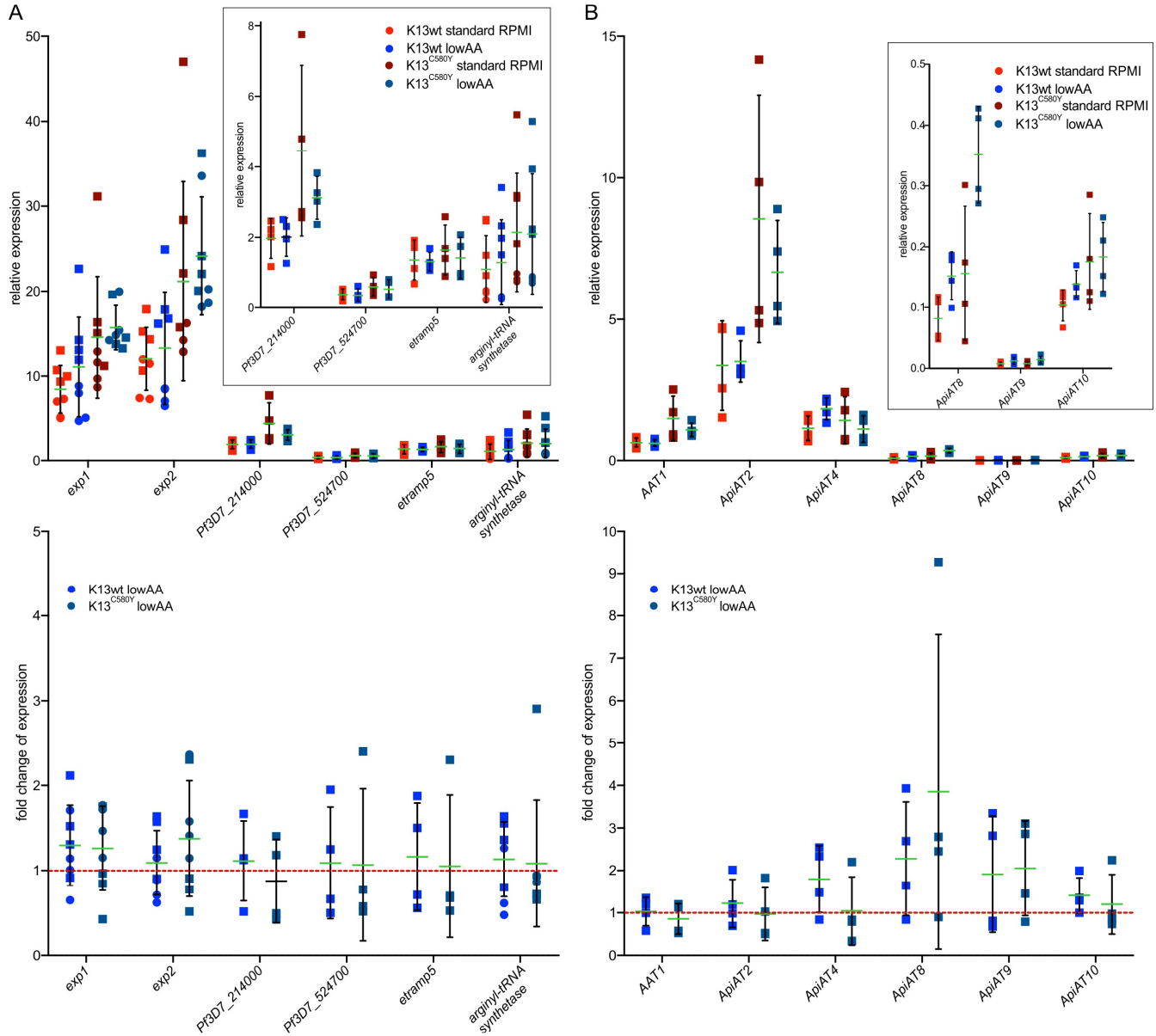


Figure S4. Gene expression in ART^R and sensitive parasites from infected humans. Related to Figure 5. (A, B) Violin plots showing the normalised expression of the indicated genes in parasites obtained from patients with the indicated parasite clearance half-life after ART treatment analysed by RNA-Seq (A) and microarrays (B). Mean of 188 samples (A) or 577 samples (B) with parasite clearance half life of <5h ($n=81$ (A) and $n=242$ (B)) (defined as non-resistant) and >5h ($n=107$ (A) and $n=335$ (B)) (defined as resistant). P values were calculated with a one sided Mann-Whitney test.



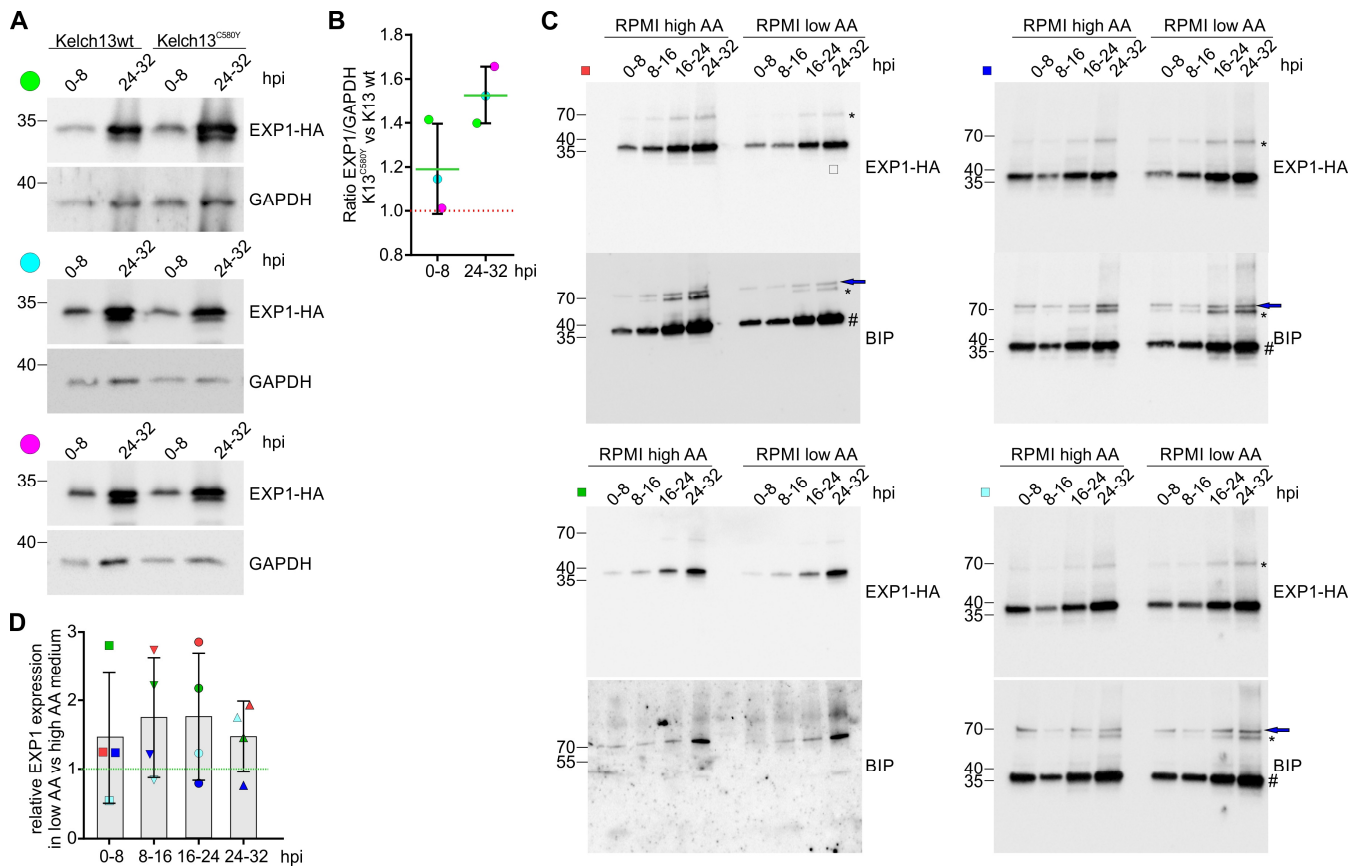


Figure S6. Densitometric analysis of EXP1 expression and eIF2 α phosphorylation. Related to Figure 5. (A) Immunoblots of protein extracts from saponin pellets from double integrant Kelch13wt+EXP1-HA and Kelch13^{C580Y}+EXP1-HA parasites harvested at the indicated time points probed with α -HA (EXP1-HA) and α -GAPDH (loading control). (B) Densitometric analysis of relative EXP1 protein expression in Kelch13^{C580Y}+EXP1-HA parasites versus Kelch13wt+EXP1-HA (red line) at the indicated time points quantified from blots shown in (A). Mean, green line. $n=3$ independent experiments (colors denote individual experiments in (A)). EXP1-HA signal was normalised to GAPDH. Data used for Figure 5G and 5H (C) Uncropped immunoblots of saponin pellets from EXP1-HA parasites grown under high and low AA conditions harvested at the indicated time points probed with α -HA (EXP1-HA) and α -BIP (loading control). $n=4$ independent experiments. Blue arrow, BIP signal; asterisk, non-skipped EXP1-HA-NeoR, see Figures S3G and S3I; hash, residual EXP1 signal after re-probing membranes. (D) Densitometric quantification of relative EXP1 protein expression in parasites grown under low AA versus high AA (green line) harvested at the indicated time points. HA signal was normalised to BIP. Values obtained from the corresponding blots (colors) shown in (C). Data used for Figure 5I and 5J. For immunoblots the marker is indicated in kDa. hpi, hours post invasion.

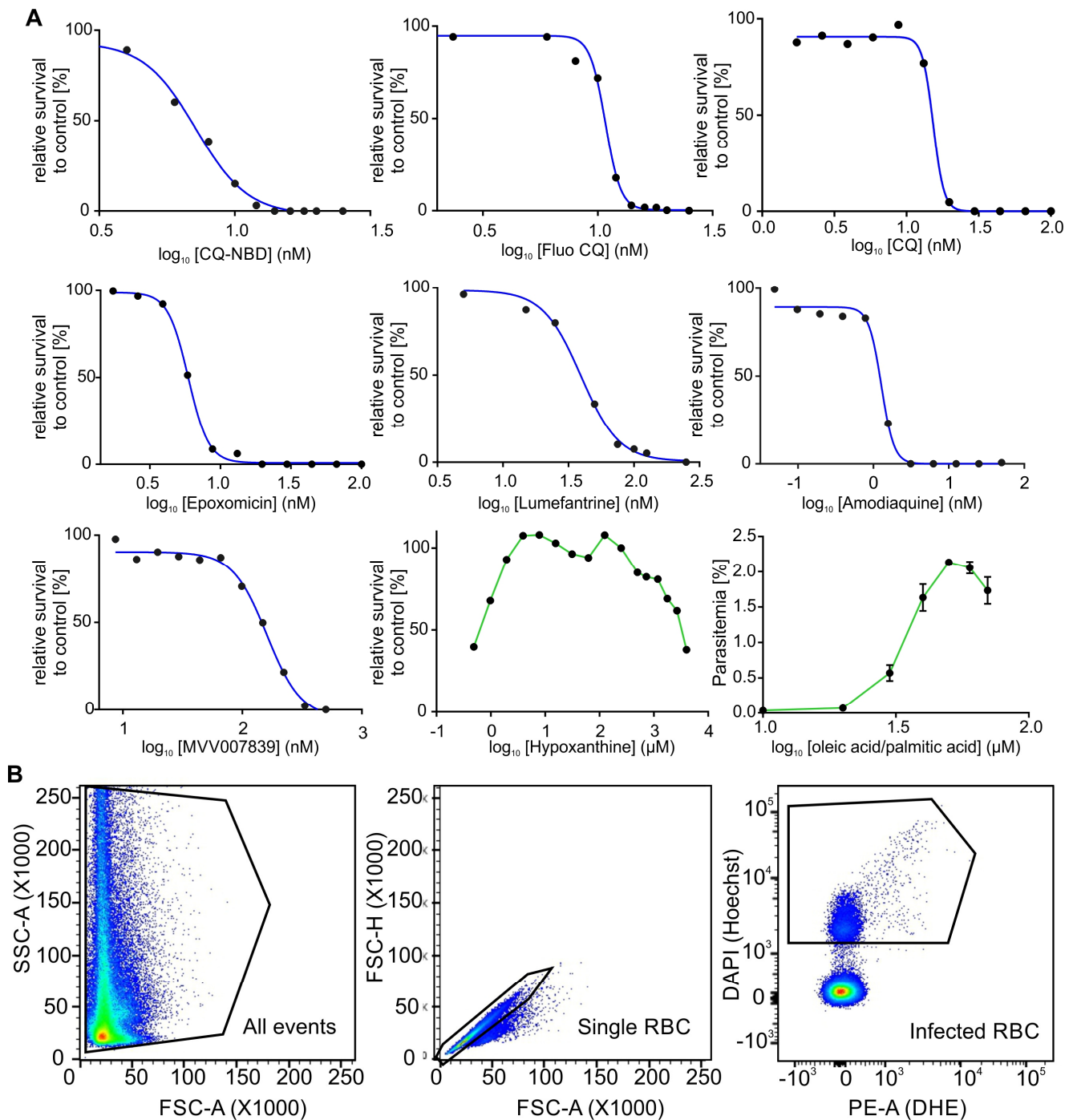


Figure S7. Determination of IC₅₀⁹⁶ for nutrients and drugs tested. Related to Figures 1 and 2.

(A) Curves of dose-dependent relative survival compared to control after 96 h of 3D7 parasites grown with increasing concentrations of the drugs and nutrients indicated (log). (B) FC gating strategy for determination of parasitemia in *P. falciparum*-infected RBC cultures. Left panel: forward versus side scatter (FSC versus SSC) plot defines population of RBCs and exclude debris. Mid panel, forward scatter height (FSC-H) versus forward scatter area (FSC-A) density plot to define single RBCs and exclude doublets. Right panel, DAPI (Hoechst) versus PE-A (dihydroethidium, DHE) density plot to distinguish infected RBCs from uninfected RBCs.